Tmc1 is necessary for normal functional maturation and survival of inner and outer hair cells in the mouse cochlea

Walter Marcotti[1], Alexandra Erven[2], Stuart L. Johnson[1], Karen P. Steel[2] and Corné J. Kros[1]

[1] *School of Life Sciences, University of Sussex, Falmer, Brighton BN1 9QG, UK*
[2] *MRC Institute of Hearing Research, University of Nottingham, Nottingham NG7 2RD, UK*

The *deafness* (*dn*) and *Beethoven* (*Bth*) mutant mice are models for profound congenital deafness (DFNB7/B11) and progressive hearing loss (DFNA36), respectively, caused by recessive and dominant mutations of transmembrane cochlear-expressed gene 1 (*TMC1*), which encodes a transmembrane protein of unknown function. In the mouse cochlea *Tmc1* is expressed in both outer (OHCs) and inner (IHCs) hair cells from early stages of development. Immature hair cells of mutant mice seem normal in appearance and biophysical properties. From around P8 for OHCs and P12 for IHCs, mutants fail to acquire (*dn*/*dn*) or show reduced expression (*Bth*/*Bth* and, to a lesser extent *Bth*/+) of the K^+ currents which contribute to their normal functional maturation (the BK-type current $I_{K,f}$ in IHCs, and the delayed rectifier $I_{K,n}$ in both cell types). Moreover, the exocytotic machinery in mutant IHCs does not develop normally as judged by the persistence of immature features of the Ca^{2+} current and exocytosis into adulthood. Mutant mice exhibited progressive hair cell damage and loss. The compound action potential (CAP) thresholds of *Bth*/+ mice were raised and correlated with the degree of hair cell loss. Homozygous mutants (*dn*/*dn* and *Bth*/*Bth*) never showed CAP responses, even at ages where many hair cells were still present in the apex of the cochlea, suggesting their hair cells never function normally. We propose that Tmc1 is involved in trafficking of molecules to the plasma membrane or serves as an intracellular regulatory signal for differentiation of immature hair cells into fully functional auditory receptors.

(Received 5 August 2005; accepted after revision 19 April 2006; first published online 20 April 2006)
Corresponding author C. J. Kros: School of Life Sciences, University of Sussex, Falmer, Brighton BN1 9QG, UK. Email: c.j.kros@sussex.ac.uk

Deafness (*dn*) is a spontaneous autosomal recessive mutation in mice that leads to a complete lack of cochlear responses (measured up to 20 days after birth) and is associated with sensory hair cell defects in homozygotes (Steel & Bock, 1980; Bock & Steel, 1983). Although spontaneous auditory nerve activity is absent in adult *dn* mice (Durham *et al.* 1989), functional connections in the central auditory pathway do occur (Bock *et al.* 1982). The semidominant *Beethoven* (*Bth*) mutation arose from an ENU (*N*-ethyl-*N*-nitrosourea) mutagenesis programme (Hrabé de Angelis *et al.* 2000) and leads to progressive hearing loss in heterozygote and early onset deafness in homozygote mice (Vreugde *et al.* 2002). Both mutations affect transmembrane cochlear-expressed gene 1 (*Tmc1*: Vreugde *et al.* 2002; *TMC1*: Kurima *et al.* 2002). Mutations in human *TMC1* cause dominant progressive hearing loss (DFNA36) and recessive profound congenital deafness (DFNB7/B11) (Kurima *et al.* 2002). *Tmc1* is a member of a novel gene family and the function of the transmembrane protein that it encodes has remained elusive (Kurima *et al.* 2002; Vreugde *et al.* 2002). Although *in situ* hybridization studies have shown that in the mouse cochlea *Tmc1* is strongly expressed in hair cells from postnatal day 5 (P5) onwards (Kurima *et al.* 2002; Vreugde *et al.* 2002), the protein is first detected just before the onset of hearing at about P10 in the pericuticular necklace and the endoplasmic reticulum (Makishima *et al.* 2005).

Functional maturation of mouse cochlear hair cells is a complex process that starts just after terminal mitosis at embryonic day 14.5 (E14.5) and lasts for about three to four weeks (Pujol *et al.* 1998). During this period, numerous morphological (Pujol *et al.* 1998) and electrophysiological (Eatock & Hurley, 2003) changes occur within the cochlea. Some of these changes are important for turning functionally immature hair cells into highly specialized sensory cells. Inner hair cells (IHCs), the primary sensory receptors of the cochlea, can fire Ca^{2+} action potentials (Kros *et al.* 1998; Marcotti *et al.* 2003*b*) before the onset of hearing, at around P10–P12 in mice

 DOI: 10.1113/jphysiol.2005.095661

(Romand, 1983). However, slow action potentials are not suited for encoding the high-frequency sounds that are typically transduced by the adult mammalian cochlea. This problem is solved in IHCs with the expression at around P12 of the large and rapidly activating BK-current $I_{K,f}$ (Kros *et al.* 1998; Marcotti *et al.* 2004*a*) and the unusually negatively activating delayed rectifier K^+ current $I_{K,n}$ (Marcotti *et al.* 2003*a*; Oliver *et al.* 2003). By reducing the cell membrane time constant, these K^+ currents allow IHCs to respond to sound with fast, graded receptor potentials. The onset of maturation in outer hair cells (OHCs), which are responsible for the amplification and tuning of auditory responses, starts from around P8 with the acquisition of both $I_{K,n}$ (Marcotti & Kros, 1999) and the electromotile activity (He *et al.* 1994; Marcotti & Kros, 1999) that is mediated by the motor protein prestin (Zheng *et al.* 2000). Since the expression of the protein encoded by *Tmc1* takes place during this period of major developmental biophysical changes in both hair cell types, we investigated whether, when mutated in *Bth* and *dn* mice, it would affect normal development of hair cell function. The relation between abnormal hair cell physiology, degeneration and hearing loss was also studied.

Methods

Mice

The *Beethoven* (*Tmc1*^{Bth}, also referred to as *Bth* below) colony was maintained on a C3HeB/FeJ background. The *deafness* (*Tmc1*^{dn}, also referred to as *dn* below) stock has been maintained on an undefined genetic background within a closed colony for over 20 years. All animal experiments were carried out in full compliance with UK Home Office regulations.

Genotyping

Primers to identify the *Tmc1*^{Bth} mutation were designed from the *Tmc1* genomic sequence. Mice from the *Beethoven* stock were genotyped using PCR to amplify a 166-bp product around the point mutation in exon 13. The primers were: 5′-GAA CAT GGT AAT GTC CCT CCT GGG CA-3′ and 5′-CTC ATC CAT CAA GGC GAG AAT GAA-3′. The primers were designed to introduce a second mutation in the PCR product, which created an *Nsp*I restriction site in the wild type; subsequent digestion gave 142 bp and 30 bp fragments from wild-type DNA and 166 bp fragments from the *Bth* allele.

The mutation in *Tmc1* in *deafness* mice is a 1.6-kb deletion (Kurima *et al.* 2002). This deletion includes all of exon 14 and part of introns 13 and 14. Primers were designed from the genomic sequence with one forward primer and two reverse primers. The primer sequence for the forward primer (5′-ATG TTC TGT CCC ACC CTG TTT GA-3′) was designed from intron 13. The sequences for reverse primer 1 (5′-CCC ACT ACA CTG TAG CCC AC-3′) and reverse primer 2 (5′-ACT ACC CAC TAC ACC CTA-3′) were designed from the *Tmc1* sequence published in Kurima *et al.* (2002). Reverse primer 2 is designed from the sequence that is created when the intron 13 and intron 14 sequences meet after the deletion has occurred. Therefore mice carrying the *dn* allele will give a PCR product of approximately 200 bp when using reverse primer 2 and the forward primer. The wild-type allele will not be amplified as the primer sequence for either intron 13 or intron 14, which is contained in reverse primer 2, will not be long enough to allow robust binding. To amplify the wild-type allele, a long-range PCR reaction is used with reverse primer 1, designed from the sequence in intron 14, and the forward primer. The amplification product is approximately 2 kb long.

Structural investigations

For scanning electron microscopy (SEM), inner ears were fixed in glutaraldehyde, the organ of Corti was exposed by dissection, and samples were processed by a modified OTOTO method (Hunter-Duvar, 1978). Cochleae were examined in *Beethoven (*number of mice at P15: 5 +/+, 6 *Bth*/+, 6 *Bth/Bth*; P30–35: 19 +/+, 21 *Bth*/+, 4 *Bth/Bth*; P60: 5 +/+, 5 *Bth*/+, 5 *Bth/Bth*) and *deafness* (P30: 5 +/*dn*, 5 *dn/dn*).

Hair cell degeneration was quantified by counting the number of normal cells and the number of degenerating cells remaining in the organ of Corti from montages of scanning electron micrographs. Three distinct areas of the cochlea were analysed: 10–20%, 40–50% and 80–90% of the total length from the base. The corresponding approximate best frequency ranges are: 47–67 kHz, 15–22 kHz and 1.3–3.2 kHz, respectively (from eqn 13 in Ehret, 1975). The areas counted were a minimum of 100 μm in length, and number of cells counted was expressed per 100 μm. Hair cells were counted from 4–7 mice at each location of each genotype at each age. Hair cells were counted as normal if their hair bundle showed the normal V- (OHCs) or crescent-shaped (IHCs) arrangement with distinct stereocilia. Hair cells were classed as degenerating or damaged if they showed any defects (viewed at a higher resolution than Figs 1*A* and 2), including missing, damaged or fused stereocilia. This method is likely to lead to an underestimation of the degenerating cells since the hair bundle structure might not be affected during early stages of cell deterioration. In fact, a previous investigation has shown that all hair cells from *deafness* mice exhibit subtler signs of degeneration in the cytoplasm and the synaptic region as early as P15 when

viewed using transmission electron microscopy, together with evidence of delayed maturation of the spaces of Nuel and tunnel of Corti by about 10 days (Bock & Steel, 1983). SEM was used here to allow quantitative comparisons of a large number of hair cells in different cochlear locations of *Beethoven* and *deafness* mice.

Cochlear electrophysiology

Mice were anaesthetized with urethane (I.P. injection using 2 mg (g body weight)$^{-1}$ as a 20% solution), a recording electrode was placed on the round window of the cochlea, and thresholds for compound action potential (CAP: a measure of the average firing activity of the afferent auditory fibres) responses determined in 2 dB steps using a standard approach (Steel & Smith, 1992). The endocochlear potential, which is the transepithelial potential of the endolymph within the cochlear duct that increases the driving force for the transducer current, was recorded using a micropipette electrode inserted into the basal turn cochlear duct through the lateral wall (Steel & Smith, 1992). Both *Beethoven* (P15: 5 +/+, 8 *Bth*/+, 6 *Bth/Bth*; P30: 9 +/+, 12 *Bth*/+, 6 *Bth/Bth*; P60: 5 +/+, 5 *Bth*/+, 5 *Bth/Bth*) and *deafness* (P30: 5 +/*dn*, 5 *dn/dn*) mice were used for this analysis.

Single-hair cell electrophysiology

Tissue preparation. Apical-coil IHCs and OHCs of *Beethoven* (*Bth*) and *deafness* (*dn*) mutant mice and their phenotypically normal controls from the same strains were studied in acutely dissected organs of Corti (ages P6–P22 for *Bth* and P7–P58 for *dn*, where the day of birth is P0). Adult and immature mice were killed by cervical dislocation, in accordance with UK Home Office regulations. The cochleae were dissected in extracellular solution composed of (mM): 135 NaCl, 5.8 KCl, 1.3 $CaCl_2$, 0.9 $MgCl_2$, 0.7 NaH_2PO_4, 5.6 D-glucose, 10 Hepes-NaOH, 2 Na-pyruvate (pH 7.5, osmolality about 306 mmol kg^{-1}). Amino acids and vitamins for Eagle's minimum essential medium (MEM) without L-glutamine were added from concentrates (Invitrogen, Paisley, UK). The organs of Corti were transferred to a microscope chamber containing extracellular solution, and immobilized under a nylon mesh. The chamber (volume 2 ml) was perfused at a flow rate of about 10 ml h^{-1} from a peristaltic pump, and mounted on the stage of an upright microscope (Zeiss ACM, Germany or Olympus, Japan). The organs of Corti were observed with Nomarski differential interference contrast optics (×40 water immersion objectives). The position of hair cells along the cochlea was calculated as percentage distance from the extreme base. In the immature cochlea, hair cells from which electrophysiological recordings were obtained were positioned at a distance of 76% to 84% from the base. Recordings in the mature cochlea were from cells positioned between 81% and 94% from the base, corresponding to a frequency range of approximately 0.8–3.0 kHz (Ehret, 1975). Tissue samples from all mice were kept for genotyping.

Electrical properties of the basolateral membrane. Hair cells (IHCs: 26 +/+, 27 *Bth*/+, 29 *Bth/Bth*, 16 +/*dn*, 28 *dn*/*dn*; OHCs: 13 +/+, 22 *Bth*/+, 30 *Bth/Bth*, 14 +/*dn*, 18 *dn*/*dn*) were whole-cell voltage clamped at room temperature (20–25°C) or near body temperature (35–37°C) using EPC-8 (HEKA, Lambrecht, Germany) or Optopatch (Cairn Research Ltd, Faversham, UK) amplifiers. Patch pipettes were pulled from soda glass capillaries (Harvard Apparatus Ltd, Edenbridge, UK) and electrode resistances in extracellular solution were 2–3 MΩ. In order to reduce the electrode capacitance, the shank of the electrode was coated with surf wax (Mr Zogs SexWax, Carpinteria, CA, USA). The normal pipette filling solution contained (mM): 131 KCl, 3 $MgCl_2$, 1 EGTA-KOH, 5 Na_2ATP, 5 Hepes-KOH, 10 Na-phosphocreatine (pH 7.3, 292 mmol kg^{-1}). Calcium currents (I_{Ca}) were recorded using the following intracellular solution to minimize contamination due to the K^+ currents (mM): 147 Cs-glutamate, 3 $MgCl_2$, 5 Na_2ATP, 0.3 Na_2GTP, 1 EGTA-NaOH, 5 Hepes-CsOH (pH 7.3, 292 mmol kg^{-1}). Data were acquired using pClamp software (Axon Instruments, Union City, CA, USA) with a LabMaster DMA or a Digidata 1320A data acquisition board. Data were filtered, depending on the protocols used, at 2.5, 5 or 10 kHz (8-pole Bessel), sampled at 5, 10 or 50 kHz and stored on computer. Offline data analysis was performed using Origin software (OriginLab, Northampton, MA, USA). For voltage-clamp experiments, current recordings were corrected offline for leak conductance (g_{leak}). In most cases g_{leak} was calculated between −84 mV and −94 mV, as the main outward K^+ currents activate positive to or around −80 mV. When the inward rectifier K^+ current (I_{K1}) was studied in immature IHCs g_{leak} was calculated in response to 10 mV hyperpolarizing voltage steps from a holding potential of −64 mV (Marcotti *et al.* 1999). Values for g_{leak} were 1.9 ± 0.1 nS ($n = 63$, P6–P8) for immature hair cells and 3.2 ± 0.3 nS ($n = 62$, P15–P58) for mature IHCs after the onset of hearing. In the experiments in which the negatively activating K^+ current ($I_{K,n}$) was studied in mature cells, g_{leak} (IHCs: 1.1 ± 0.1 nS, $n = 36$; OHCs: 1.2 ± 0.1 nS, $n = 49$) was measured at very hyperpolarized potentials at which $I_{K,n}$ was deactivated (Marcotti & Kros, 1999; Marcotti *et al.* 2003*a*). Residual series resistance (R_s) after compensation (50–90%) was 2.5 ± 0.1 MΩ (range 0.4–9.8 MΩ, $n = 223$). Membrane potentials under voltage clamp were corrected for the voltage drop across the residual R_s at steady-state current level and for a liquid junction potential, measured between pipette and bath solutions, of −4 mV for the KCl-based and

−11 mV for the Cs-glutamate-based intracellular solution. For current-clamp experiments, offline series resistance correction was applied only if the voltage drop exceeded 1 mV. For voltage-clamp recordings, the holding currents were plotted as zero current unless otherwise specified.

Mechano-electrical transducer currents. Mechano-electrical transducer currents were elicited in apical-coil OHCs (P6–P8) from *Bth* and *dn* mutant mice, using a fluid jet driven by a piezoelectric disc and recorded under whole-cell voltage clamp as previously described (Kros *et al.* 1992). Mechanical stimuli were applied using 45 Hz sinusoids with a driver-voltage amplitude of 35 V, resulting in saturating transducer currents (filtered at 1 kHz, 8-pole Bessel). Although bundle movements were not recorded for this study, the corresponding bundle displacements should be in the order of 150–200 nm (Géléoc *et al.* 1997; Marcotti *et al.* 2005). Data were acquired using Asyst software (Keithley Instruments, Rochester, NY, USA), filtered at 2.5 kHz, sampled at 5 kHz and stored on computer for off-line analysis using Origin software. For these experiments, no correction was made for the voltage drop across R_s, which was at most 4 mV at extreme potentials.

Membrane capacitance measurements. Real-time changes in membrane capacitance (ΔC_m) were studied under voltage clamp at 37°C and measured using the track-in mode of the Optopatch (Johnson *et al.* 2002; 2005) in both *Beethoven* (P16–P17, $n = 13$) and *deafness* (P17–P18, $n = 9$) apical-coil IHCs. Simultaneous recordings of ΔC_m and Ca^{2+} currents were performed using the same intracellular solutions used for I_{Ca} measurements (see above). A 2.5 kHz sine wave of 18.5 mV amplitude was applied to IHCs from a holding potential of −81 mV using the internal oscillator of the Optopatch. The sine wave was small enough not to activate any significant membrane current, since accurate membrane capacitance calculation requires a high and constant membrane resistance. The command sine wave was interrupted for the duration of the voltage steps so inward currents could be recorded. The capacitance signal from the Optopatch was amplified (×50), 2-pole filtered at 150 Hz with additional 8-pole Bessel filtering at 250 Hz, and sampled at 5 kHz. During multiple step protocols, the prestimulus C_m baseline for consecutive steps was set to zero during offline analysis. IHCs were stimulated using voltage steps of 100 ms duration from the holding potential of −81 mV to more positive potentials in 10 mV increments. Changes in membrane capacitance were calculated by subtracting the mean capacitance measured over a 300 ms period, starting at around 50 ms after the end of the voltage step, from the mean prepulse capacitance (averaged over a 200 ms period). We allowed approximately 5–10 s per stimulus for vesicle pool replenishment.

Extracellular superfusion. Acetylcholine (Sigma, Gillingham, UK), at a concentration of 100 μM, was used to assess the presence of the small-conductance Ca^{2+}-activated K^+ current I_{SK} (Evans, 1996; He & Dallos, 1999; Glowatzki & Fuchs, 2000; Katz *et al.* 2004; Marcotti *et al.* 2004*b*) in mature OHCs and IHCs. Ca^{2+}-free extracellular solutions contained 0.5 mM EGTA, and Mg^{2+} was increased to 3.9 mM to minimize changes in membrane charge screening. ΔC_m and I_{Ca} were recorded during the superfusion of 30 mM TEA (Fluka, Gillingham, UK) to block most of the IHC K^+ currents. In this solution, NaCl was reduced to keep the osmolality constant. Solutions were applied via a multibarrelled pipette positioned close to the hair cells, so that solution changes were almost instantaneous (dead space within the perfusion pipette is about 1 μl).

Statistical analysis

Statistical comparisons of means were made using Student's two-tailed *t* test or, for comparisons of multiple data sets, one-way ANOVA (followed by the Tukey post test). Two-way ANOVA, followed by the Bonferroni test, was used to compare CAP thresholds. For all statistical tests $P < 0.05$ was used as the criterion for statistical significance and mean values are quoted ± standard error (S.E.M.) in text and figures. In all figures, statistically significant difference is indicated by asterisks.

Results

Ultrastructural observations and cochlear function in *deafness* and *Beethoven* mutants

Deafness homozygotes (*dn*/*dn*) at P30 showed significant hair cell damage and loss in the middle (40–50%) and basal (10–20%) turns of the cochlea (Fig. 1*A* and *C*) compared to heterozygous controls (+/*dn*). In the apical region, many (80–90%) hair cells retained a normal, or near-normal, bundle appearance in *dn*/*dn* mice (Fig. 1*A*). Cells from a similar apical, low-frequency region were selected to study the developmental maturation of the biophysical properties of both IHCs and OHCs, to minimize the confounding factor of hair cell degeneration (see below). The physiological consequences of these hair cell defects were investigated in anaesthetized mice by measuring CAP thresholds. A previous investigation had shown that homozygous *deafness* mice lacked any cochlear responses (CAP, summating potentials and cochlear microphonics) to sound stimuli between the ages of P12 and P20 (Steel & Bock, 1980; Bock & Steel, 1983). In the present study we found that also at P30 no CAP responses could be elicited in homozygous *deafness* mice, even at the maximum sound intensity used over the entire frequency range

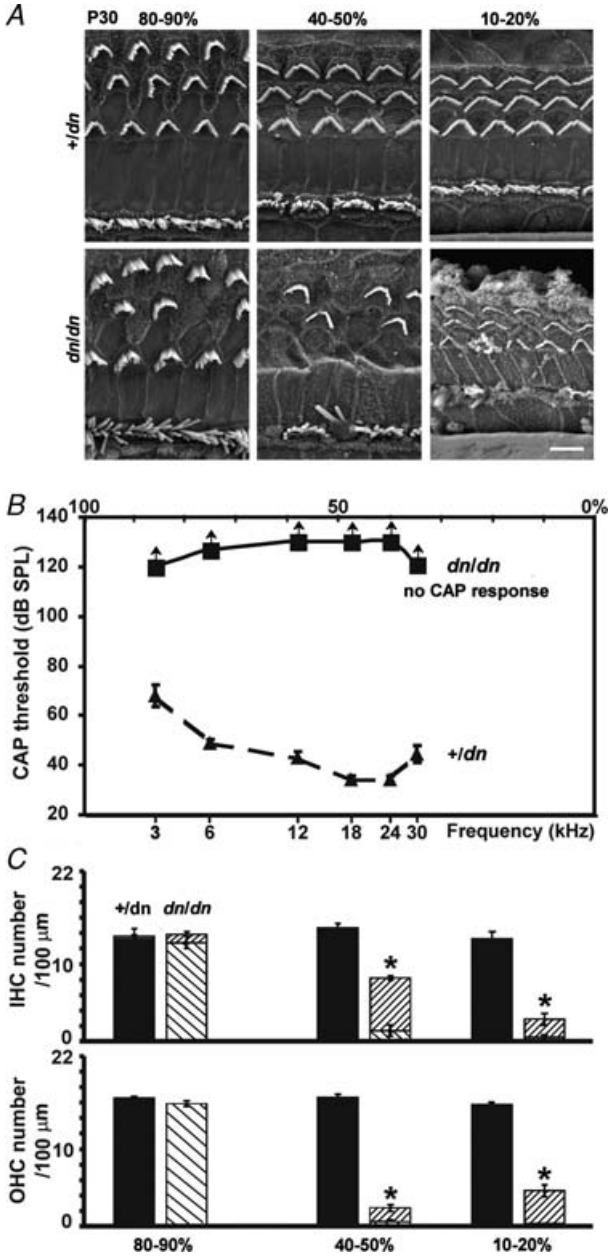

Figure 1. Morphological and physiological properties of *deafness* cochleae
A, low-resolution scanning electron micrographs (SEM) from the apical (80–90%), middle (40–50%) and basal (10–20%) regions of P30 +/*dn* and *dn*/*dn* cochleae, showing the three rows of V-shaped hair bundles of OHCs and one row of crescent-shaped bundles of IHCs. Hair cell degeneration in *dn*/*dn* only appears to be present in the 40–50% and 10–20% regions. Scale bar represents 5 μm. *B*, mean compound action potential (CAP) thresholds in +/*dn* (▲) and *dn*/*dn* (■) mice aged P30. The *dn*/*dn* mice showed no CAP response at the maximum sound intensities that could be used, which is represented with arrows pointing upwards. Sound frequency (lower axis) is scaled tonotopically as percentage distance (upper axis) from the base (calculated from Ehret, 1975). *C*, hair cell counts, using high-resolution SEM, per 100 μm in the same three relevant areas of P30 mouse cochleae described in *A*. Filled and diagonally striped bars (\) represent normal hair cells observed in the +/*dn* and *dn*/*dn* cochlea, respectively. The more densely striped bars (/) represent degenerating hair cells.

tested (between 3 and 30 kHz), while heterozygotes showed normal thresholds (Fig. 1*B*). The absence of cochlear responses at low frequencies (3 and 6 kHz), despite the presence of apical-turn hair cells, suggests that these cells

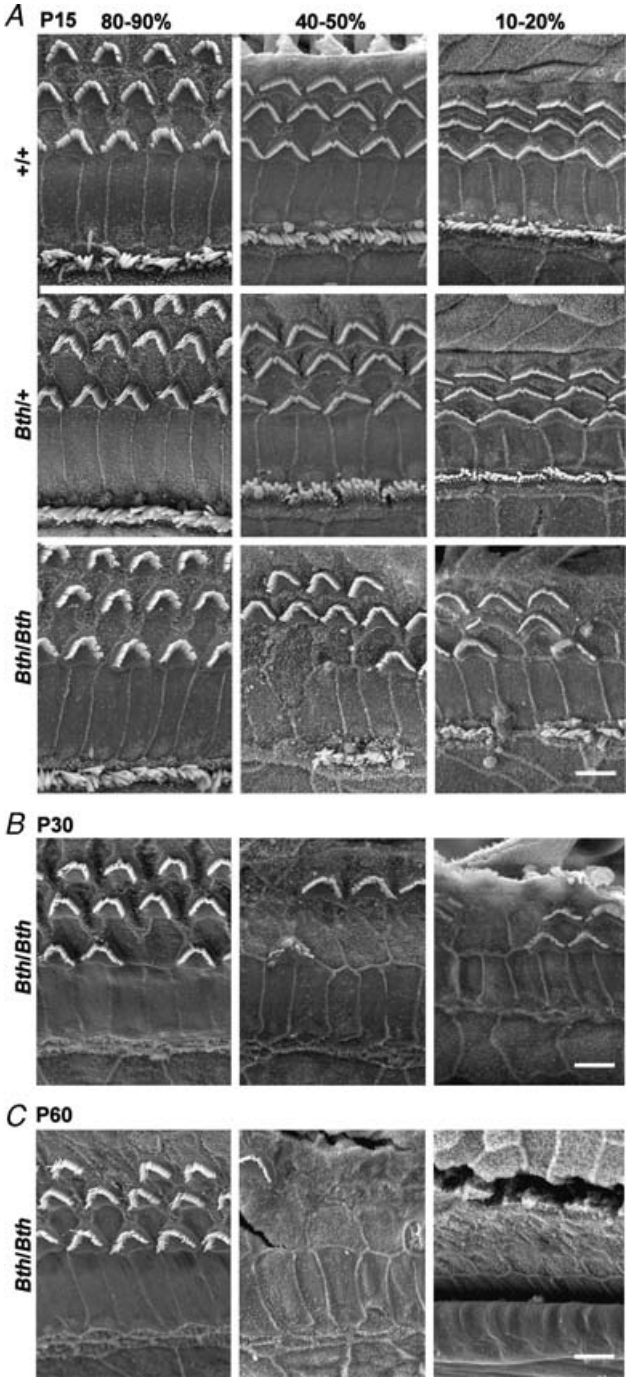

Figure 2. Morphological characteristics of *Beethoven* cochleae
A, low-resolution SEM of +/+, *Bth*/+ and *Bth*/*Bth* at P15 from the same three cochlear regions as in Fig. 1*A*. *B* and *C*, SEM of *Bth*/*Bth* at P30 and P60, respectively. *Bth*/*Bth* cochleae show degeneration of both hair cell types in the 40–50% and 10–20% regions at all ages. No clear signs of degeneration were observed in the apical region (80–90%) of P15 *Bth*/*Bth*, or in any region of P15 *Bth*/+ cochleae. Scale bar represents 5 μm.

are not functioning normally even before they degenerate. Hence, the observed loss and profound degeneration of hair cells in the middle and basal region of the cochlea is likely to be a secondary consequence and not the primary cause of deafness in *dn/dn* mutants.

Beethoven homozygotes (*Bth*/*Bth*) showed hair cell damage and a significant reduction in the number of cells in the basal and middle turns by P15, but no significant hair cell loss in the apical region (Figs 2*A* and 3*A*, lower panel). The loss of hair cells in *Beethoven* homozygotes was even greater at P30 (Fig. 2*B* and Vreugde *et al.* 2002) and P60 (Figs 2*C* and 3*B*, lower panel), with an unusual pattern in that IHCs were being lost at an earlier age than OHCs. In the apical turns of homozygotes at these older

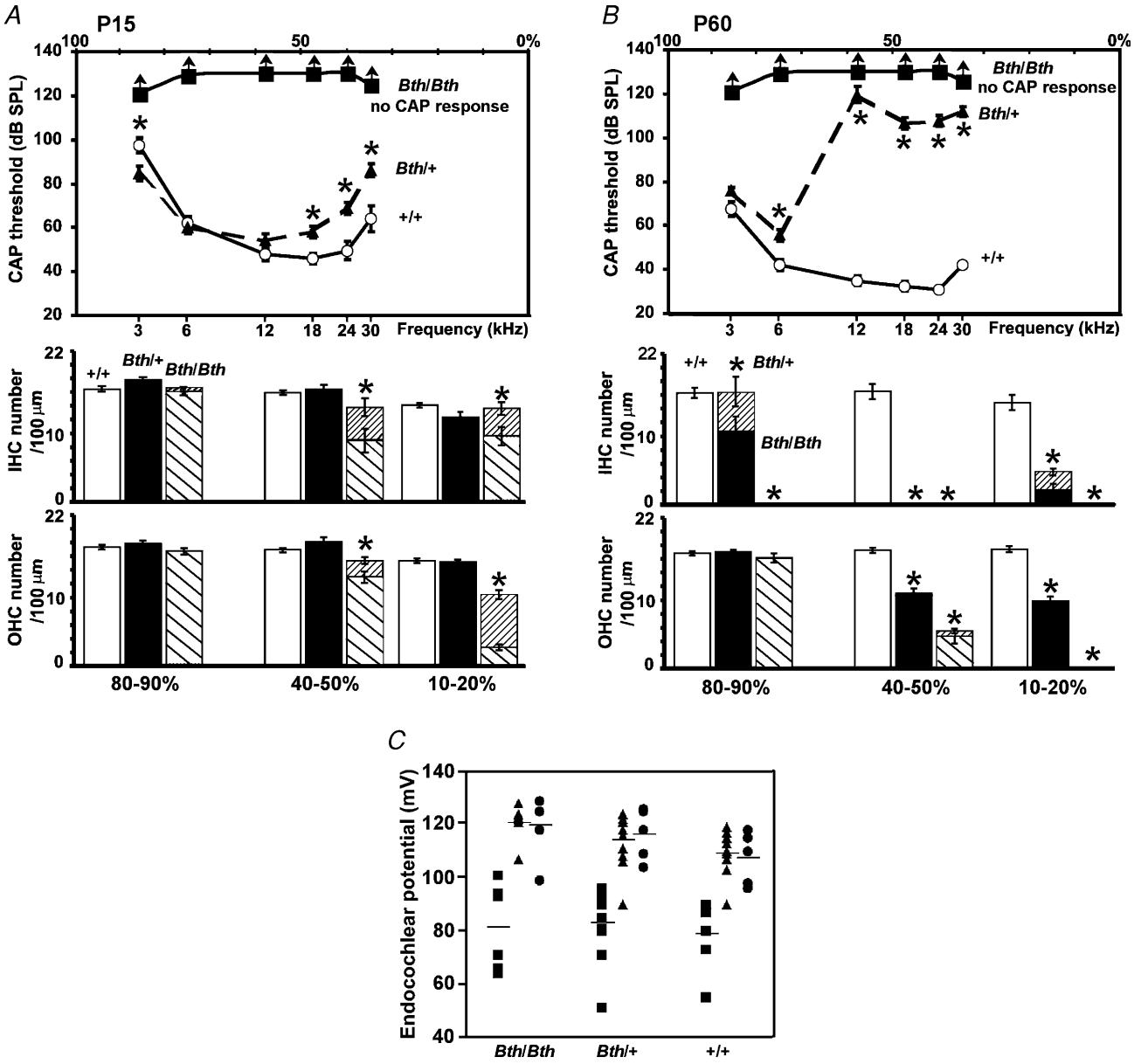

Figure 3. Physiological properties and hair cell survival of *Beethoven* cochleae
A and *B*, average CAP (top panels) and hair cell counts per 100 μm of the cochlear coil using high-resolution SEM (bottom panels) in +/+, *Bth*/+ and *Bth*/*Bth* mice at P15 and P60, respectively. The arrows shown for CAP responses in *Bth*/*Bth* mice indicate that the actual thresholds could not be measured because they must have been higher than the maximum sound intensities used (■). The open bars shown in *A* and *B* (bottom panels) represent normal hair cells observed in the +/+ cochlea; filled bars are the normal cells in the *Bth*/+ cochlea, the striped bars (\) indicate normal cells in the *Bth*/*Bth* cochlea and the more densely striped bars (/) represent degenerating hair cells in all genotypes. *C*, endocochlear potential measured in *Beethoven* mice at P15 (■), P30 (▲) and P60 (●). Horizontal lines represent the mean values of endocochlear potential at each age.

ages, there were stretches with no IHCs remaining, but a complete complement of OHCs. This pattern of hair cell loss clearly differs from that in *dn*/*dn* mice, where IHCs and OHCs appear equally affected (Fig. 1*C*). In contrast to the complete lack of cochlear responses in *dn/dn* mice, *Bth/Bth* mice showed summating potential responses, both positive and negative, to sound (data not shown), suggesting some hair cell function *in vivo*. However, no CAP responses up to the maximum sound intensity used could be recorded in homozygous *Beethoven* mutant mice at P15 (Fig. 3*A*), P30 (not shown) and P60 (Fig. 3*B*). Similar to our findings in *dn*/*dn* mice (Fig. 1), the limited extent of hair cell degeneration in the apical turn of the cochlea in *Bth/Bth* mice did not seem to correlate with the absence of CAP responses already evident at P15, suggesting again that hair cell death alone is not sufficient to explain the lack of cochlear responsiveness.

In the *Beethoven* heterozygous (*Bth*/+) mutant mice at P15, there was no obvious hair cell damage or loss in any cochlear turn (Figs 2*A* and 3*A*, lower panel), even though there was already a small but significant elevation of CAP thresholds compared to wild-type mice of the same genetic background (+/+) for frequencies of 18 kHz and higher (Fig. 3*A*, top panel). However, hair cell degeneration was evident in *Bth*/+ at P30 (Vreugde *et al.* 2002). A large increase in CAP threshold was observed in *Bth*/+ at P30 for frequencies of 12 kHz and above (previously reported by Vreugde *et al.* 2002) with a further worsening by P60 when the 6 kHz threshold was also raised (Fig. 3*B*, top panel). By contrast, wild-type mice from the *Beethoven* colony showed some improvement in CAP thresholds from P15 to P60 associated with maturation (Fig. 3*A* and *B*, top panels). *Beethoven* heterozygotes (*Bth*/+) had by P60 a similar pattern of hair cell loss as the *Bth/Bth* homozygotes, with IHC loss being more pronounced than OHC loss, but the process was delayed in heterozygotes compared with the homozygotes. Endocochlear potentials are present and entirely normal in *Beethoven* homozygotes and heterozygotes, increasing in size between P15 and P30 as the potential matures (Fig. 3*C*). Size and developmental time course of the endocochlear potential were also normal in *dn/dn* mice (Bock & Steel, 1983). Of the three types of mutant tested in this study, only *Bth*/+ showed a clear correlation between hair cell loss and raised CAP thresholds. Therefore in the *Beethoven* heterozygotes the hearing loss might be a consequence of hair cell loss, whereas in the *Beethoven* and *deafness* homozygotes a more profound functional problem might underlie the deafness. This hypothesis prompted us to investigate the physiological properties of auditory hair cells in the three mutants, since the two homozygotes might show abnormalities in their physiological development not detected in the *Beethoven* heterozygotes (Vreugde *et al.* 2002).

Deafness and *Beethoven* outer hair cells have large mechano-electrical transducer currents

The lack of cochlear microphonics (recorded between P12 and P20) in the presence of normal endocochlear potentials in *dn*/*dn* mice has prompted speculation that Tmc1 might be the mechano-electrical transducer channel (Steel & Bock, 1980; Kurima *et al.* 2002). Therefore we first sought to establish whether mechano-electrical transduction was functional in these mutants. OHCs only were studied because their transducer currents could be more conveniently recorded than those of IHCs, and because the contribution of IHCs to the cochlear microphonic is thought to be small (Dallos *et al.* 1972). Transducer currents in apical-coil OHCs (P6–P8) from both *Beethoven* and *deafness* control and mutant mice were elicited by alternating inhibitory and excitatory bundle displacements using sinusoidal force stimuli (Kros *et al.* 1992). When saturating excitatory stimuli were applied to the bundle, large transducer currents, up to about −1500 pA at −104 mV and in 1.3 mM extracellular Ca^{2+}, could be recorded in both *deafness* (+/*dn* and *dn*/*dn*) and *Beethoven* (+/+, *Bth*/+ and *Bth*/*Bth*) OHCs. Figure 4*A* and *B* shows examples of mechano-electrical transducer currents recorded from heterozygous control (+/*dn*) and homozygous (*dn*/*dn*) *deafness* OHCs at P8, which in the mouse corresponds to their onset of functional maturation (Marcotti & Kros, 1999). At negative membrane potentials, large inward transducer currents were elicited upon moving the bundles towards the kinocilium in the excitatory direction. When the bundles were moved in the inhibitory direction any transducer channels open in the absence of mechanical stimulation (normally about 5–10%) were closed, resulting in a reduction of the inward current. Starting from −104 mV and stepping the membrane potential to more depolarized values, the transducer currents decreased in size at first, and then reversed near 0 mV in both +/*dn* (+4.6 ± 1.3 mV, $n = 4$) and *dn/dn* (+4.0 ± 0.5 mV, $n = 6$) OHCs, commensurate with the currents flowing through non-selective cation channels (Ohmori, 1985). For membrane potentials positive to this reversal potential, fluid jet stimuli in the excitatory direction now caused outward currents. Figure 4*C* and *D* shows the size of the transducer current recorded at −104 mV and +96 mV in both *deafness* (controls: +/*dn;* mutants: *dn*/*dn*) and *Beethoven* (controls: +/+; mutants: *Bth*/+ and *Bth*/*Bth*) OHCs, respectively, when saturating sinusoidal stimuli were applied to the bundle. The pooled average current sizes, recorded from OHCs at immature stages (P6–P7) and at their onset of maturation (P8), did not differ significantly between controls and mutants in both *Beethoven* (see also Vreugde *et al.* 2002) and *deafness* OHCs. The resting open probability of the transducer channels in +/*dn* OHCs increased from 5.6 ± 1.7% at −104 mV to 31.6 ± 6.1%

at +96 mV ($n = 4$, P7–P8). Recordings from *dn*/*dn* cells yielded similar values (−104 mV: 5.0 ± 0.5%; +96 mV: 33.6 ± 4.0%, P7–P8, $n = 6$). Similar entirely normal shifts in resting open probability upon depolarization were found in *Beethoven* OHCs (P6–P8). The larger open probability at positive membrane potentials reflects an increased resting tension on the transducer channels due to the smaller driving force for Ca^{2+} influx reducing adaptation (Crawford *et al.* 1989).

OHCs from *deafness* mice fail to develop adult-type basolateral ion channels

Since the transducer current recorded from OHCs (+/*dn* and *dn*/*dn*) during either immature stages (P6–P7) or at their onset of functional maturation (P8) appeared unaffected by the mutation in *Tmc1*, we investigated whether basolateral membrane currents expressed by hair cells were altered. Typical examples of K^+ currents recorded from +/*dn* and *dn*/*dn* immature (P7) OHCs are shown in Fig. 5*A* and *B*, respectively. Voltage steps positive to about −50 mV caused the activation of voltage-dependent outward currents (a delayed rectifier-type K^+ current named $I_{K,neo}$, Kros *et al.* 1998) in all OHCs investigated. The size of $I_{K,neo}$, measured at 160 ms and at 0 mV, was not significantly different between control and mutant OHCs (Fig. 5*C*). The activation curve and the activation kinetics of $I_{K,neo}$ were also similar between mutant and control OHCs and to those found in normal age-matched CD-1 mice (Marcotti & Kros, 1999). Although we did not analyse I_{Ca} in immature OHCs in isolation, its presence was evident from the small inward currents preceding the much slower outward $I_{K,neo}$ in both +/*dn* and *dn*/*dn* cells (Fig. 5*A* and *B*, arrows). Moreover, *dn*/*dn* OHCs showed similar resting membrane potentials and linear leak conductance as +/*dn* controls, suggesting the absence of cell degeneration during immature stages of development. These results indicate that immature OHCs are unlikely to be affected by the mutation in *Tmc1*.

The onset of functional maturation in mouse OHCs starts at P8 with the acquisition of both the slow delayed rectifier K^+ current $I_{K,n}$, which has a hyperpolarized activation range starting from −136 mV (calculated as 5% of the maximum activation), and electromotility (Marcotti & Kros, 1999). Figure 5*D* shows typical current recordings from a control heterozygous (+/*dn*) P8 OHC. Hyperpolarizing voltage steps from a holding potential of −84 mV elicited an inward K^+ current that commenced instantaneously and decayed slowly to a steady-state level, indicating deactivation of channels that were open at the holding potential, similar to previously described results in OHCs for $I_{K,n}$ of normal CD-1 mice (Marcotti & Kros, 1999). Depolarizing voltage steps elicited $I_{K,neo}$ in addition to $I_{K,n}$. When the same voltage protocol was applied to *dn*/*dn* P8 OHCs, only $I_{K,neo}$ was evident (Fig. 5*E*). The absence of $I_{K,n}$ in *dn*/*dn* cells was even more evident at later stages of development (Fig. 5*G*) when OHCs

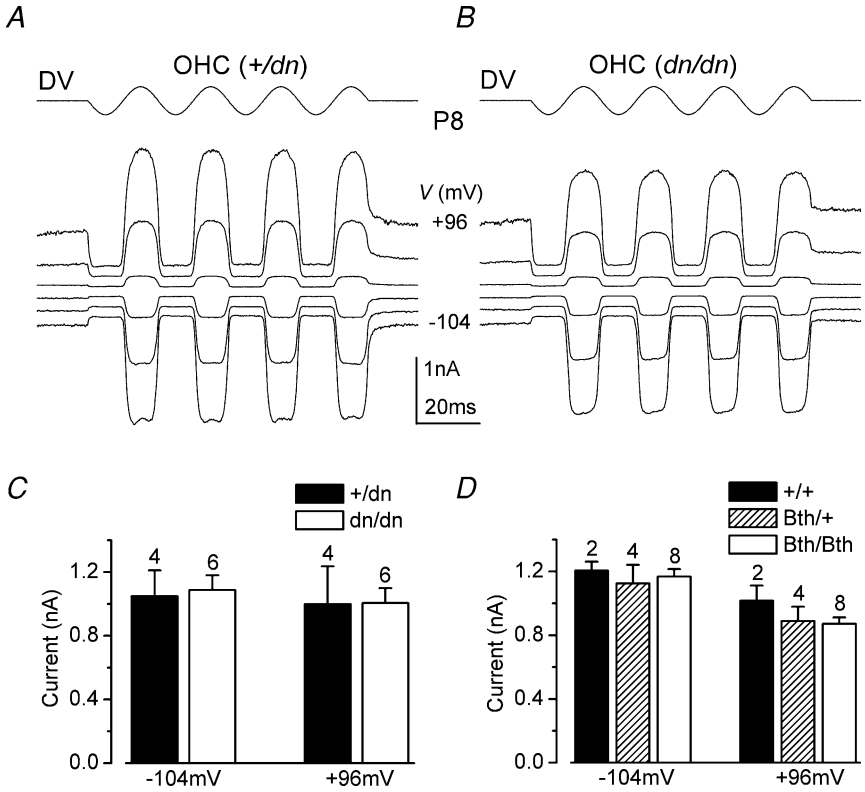

Figure 4. Mechano-electrical transducer currents in *deafness* and *Beethoven* mutant mice
A and *B*, transducer currents recorded from a control +/*dn* (*A*) and a mutant *dn*/*dn* (*B*) OHC (P8, apical coil) by applying sinusoidal force stimuli of 45 Hz. Driver voltage signal (DV; amplitude 35 V) to the fluid jet is shown above the traces. Positive deflections of the DV are excitatory. The cells were held at −84 mV, and the membrane potential was stepped between −104 mV and +96 mV in 20 mV increments. For clarity, only responses to every other voltage step are shown. Current recordings in this and in the following figures are single traces unless otherwise stated. Traces in *A* and *B* are offset so that the zero-transducer current levels (responses to inhibitory stimuli) are equally spaced. +/*dn*: C_m 6.3 pF, R_s 1.2 MΩ. *dn*/*dn*: C_m 5.8 pF, R_s 2.5 MΩ. Bundle height for both cells 4 μm. *C* and *D*, absolute size of the transducer current, using saturating stimuli, at membrane potentials of −104 mV and + 96 mV in *dn* (*C*) and *Bth* (*D*) controls and mutant mice. All recordings were at room temperature.

from +/*dn* (Fig. 5*F*) and normal CD-1 mice (Marcotti & Kros, 1999) expressed a large $I_{K,n}$. The small remaining outward K^+ current in *dn*/*dn* OHCs (I_K) activates from a much more depolarized potential (about −48 mV: 5% of the maximum activation) than $I_{K,n}$. This current was previously observed in normal CD-1 mice upon abolishing $I_{K,n}$ with a fully blocking concentration of linopirdine (Marcotti & Kros, 1999). It is possible that I_K is simply a downregulated version of $I_{K,neo}$, but this remains to be investigated in detail. The maximum size of $I_{K,n}$ in control and mutant cells at P14 (Fig. 5*H*) was measured as the deactivating current at −124 mV

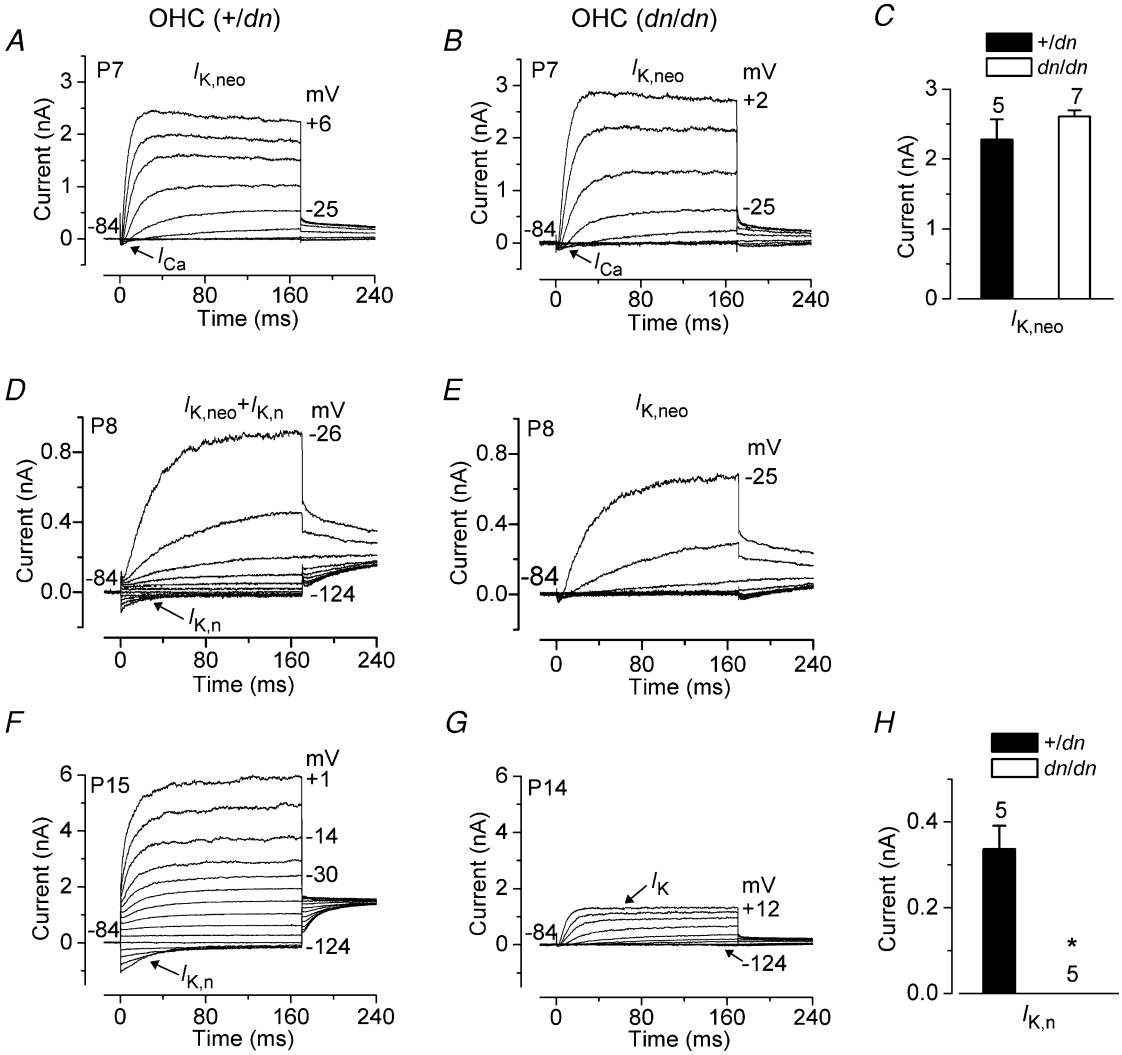

Figure 5. K^+ currents in OHCs from *deafness* mutant mice
A and *B*, total current recorded from a control (*A*, +/*dn*) and a mutant (*B*, *dn*/*dn*) P7 apical-coil OHC. Membrane currents were elicited in response to depolarizing voltage steps (10 mV increments) from −104 mV to the various test potentials shown by some of the traces, starting from the holding potential of −84 mV. In this and in the following figure (panels *A* and *B*), arrows indicate the presence of the inward Ca^{2+} currents in immature IHCs. +/*dn:* V_m −68 mV; C_m 6.6 pF; R_s 4.1 MΩ; g_{leak} 1.5 nS; *dn*/*dn:* V_m −69 mV; C_m 6.3 pF; R_s 1.5 MΩ; g_{leak} 2.6 nS. *C*, size of $I_{K,neo}$ measured at 160 ms and at 0 mV in both +/*dn* and *dn*/*dn* apical OHCs. *D* and *E*, typical membrane currents recorded from +/*dn* (*D*) and *dn*/*dn* (*E*) P8 apical-coil OHCs. Currents were elicited by applying depolarizing voltage steps in 10 mV increments starting from −124 mV from the holding potential of −84 mV. Note the absence of the negatively activating K^+ current $I_{K,n}$ in the *dn*/*dn* OHC (*E*). +/*dn:* V_m −72 mV; C_m 5.8 pF; R_s 1.8 MΩ; g_{leak} 1.8 nS; *dn*/*dn:* V_m −66 mV; C_m 5.7 pF; R_s 1.4 MΩ; g_{leak} 1.7 nS. *F* and *G*, membrane currents recorded from +/*dn* (P15) and *dn*/*dn* (P14) OHCs, respectively. Voltage protocol as in *D* and *E*. $I_{K,n}$ was absent in *dn*/*dn* OHCs, leaving only the small delayed rectifier I_K. +/*dn*: V_m −79 mV; C_m 10.8 pF; R_s 2.5 MΩ; g_{leak} 2.0 nS. *dn*/*dn*: V_m −66 mV; C_m 8.2 pF; R_s 2.8 MΩ; g_{leak} 1.6 nS. *H*, size of $I_{K,n}$ measured as the difference between instantaneous and steady-state deactivating tail currents for voltage steps from −84 mV to −124 mV in +/*dn* ($n = 5$, P14–P15) and *dn*/*dn* ($n = 5$, P14) mice. All recordings were at room temperature.

(difference between instantaneous and steady-state inward currents).

Since the expression of $I_{K,n}$ in OHCs from normal CD-1 mice coincides with the appearance of the cells' electromotile activity from about P8 onwards (Marcotti & Kros, 1999), we tried to investigate whether electromotility was also affected by the mutation. Despite the absence of $I_{K,n}$, *dn*/*dn* OHCs (P19, $n = 3$) exhibited clear electromotile activity that was visualized under the experimental microscope when cells were depolarized from the holding potential of −64 mV (Marcotti & Kros, 1999). Non-linear capacitance was also evident in the current recordings. After reaching the whole-cell configuration, adult mutant OHCs appeared to be quite fragile, and usually only lasted long enough to record a few voltage-clamp protocols. This short lifetime prevented us from successfully measuring the displacements, so any modest reduction in electromotility may have gone undetected.

Adult-type basolateral ion channels are missing in IHCs from *deafness* mice

IHCs start to mature a few days later than OHCs, at around the onset of hearing at P12, with the acquisition of a rapidly activating large-conductance Ca^{2+}-activated K^+ current ($I_{K,f}$, Kros *et al.* 1998; Marcotti *et al.* 2003*a*) and a smaller $I_{K,n}$ (Marcotti *et al.* 2003*a*; Oliver *et al.* 2003). Before P12, mouse IHCs express a variety of basolateral membrane currents, some of which are only transiently present during immature stages of development (Marcotti *et al.* 1999, 2003*b*, 2004*b*). Figure 6*A* and *B* shows typical outward K^+ current ($I_{K,neo}$) recordings from P7 +/*dn* and *dn*/*dn* IHCs. The activation kinetics, activation curve and size (Fig. 6*C*) of $I_{K,neo}$ were similar between control and mutant cells and to those found in normal age-matched CD-1 mice (Marcotti *et al.* 2003*a*). The size of the inward-rectifier K^+ current (I_{K1}), measured at −154 mV (recordings not shown), was also similar between mutant (−472 ± 72 pA, $n = 3$) and control (−441 ± 42 pA, $n = 4$) IHCs (Fig. 6*C*). The presence of I_{Ca} in immature IHCs was seen as a small, rapidly activating inward current preceding the much slower outward $I_{K,neo}$ in all +/*dn* and *dn*/*dn* cells investigated (Fig. 6*A* and *B*). The peak I_{Ca}, measured at room temperature and using 1.3 mM extracellular Ca^{2+}, occurred at around −20 mV, and was similar between +/*dn* controls (−265 ± 63 pA, $n = 4$) and mutant *dn*/*dn* (−225 ± 24 pA, $n = 7$) IHCs. These results suggest that mutations in *Tmc1* did not prevent the normal physiological development of prehearing IHCs.

Figure 6*D* and *E* shows the total outward K^+ current recorded in adult IHCs from control (+/*dn*) and mutant (*dn*/*dn*) mice, respectively. In +/*dn* IHCs (P18–P58, $n = 8$) depolarizing voltage steps caused the rapid activation of outward K^+ currents similar to those recorded in adult CD-1 mice (Kros *et al.* 1998; Marcotti *et al.* 2004*a*). These currents are mainly composed of $I_{K,f}$ and a much slower delayed-rectifier current ($I_{K,s}$) which develops from the immature $I_{K,neo}$ (Marcotti *et al.* 2003*a*). When the same voltage protocol was applied to *dn*/*dn* IHCs (P17–P58, $n = 14$), the total outward K^+ current was smaller and activated more slowly (Fig. 6*E*), suggesting that $I_{K,f}$ is likely to be absent in these mutant cells. The different activation time course between +/*dn* and *dn*/*dn* IHCs is more evident when the current onsets are displayed on an expanded time scale (Fig 6*D* and *E*, insets). The size of the total steady-state current ($I_{K,f} + I_{K,s}$), measured at 160 ms and at −25 mV, was found to be significantly larger ($P < 0.001$) in +/*dn* than in *dn*/*dn* IHCs (Fig. 6*F*). To find out whether $I_{K,f}$ was indeed absent in *dn*/*dn* IHCs, we measured its size in isolation (at 1.5–3.0 ms from the start of the voltage steps) at a membrane potential of −25 mV. This time range was selected because the rapidly activating $I_{K,f}$ had nearly reached its steady-state, while the slower $I_{K,s}$ was only just beginning to activate (Kros *et al.* 1998; Marcotti *et al.* 2004*a*). Figure 6*F* shows that $I_{K,f}$ was absent in *dn*/*dn* cells, whereas $I_{K,s}$, obtained by subtracting any $I_{K,f}$ from the total current, was present and of normal size.

The next step was to verify whether $I_{K,n}$, the other K^+ current characteristic of adult IHCs, was also absent in mutant IHCs, as was the case for *dn*/*dn* OHCs (Fig. 5*E* and *G*). In IHCs of +/*dn* mice, hyperpolarizing voltage steps from a holding potential of −64 mV elicited inward K^+ currents that commenced instantaneously and decayed slowly to a steady-state level (Fig. 6*G*), indicating deactivation of $I_{K,n}$ that was similar to that found in IHCs of CD^{-1} mice (Marcotti *et al.* 2003*a*; Oliver *et al.* 2003). $I_{K,n}$ from IHCs was recorded from −64 mV instead of −84 mV as for OHCs (Fig. 5*D* and *F*), to allow comparisons with previous results recorded from IHCs of CD-1 mice (Marcotti *et al.* 2003*a*). Depolarizing voltage steps elicited $I_{K,f}$ and $I_{K,s}$ in addition to $I_{K,n}$. When the same voltage protocol consisting of hyperpolarizing and depolarizing voltage steps was applied to *dn*/*dn* IHCs, only $I_{K,s}$ was evident (Fig. 6*H*). The maximum size of $I_{K,n}$ in control and mutant IHCs (Fig. 6*I*) was measured as the deactivating current at −124 mV from the holding potential of −64 mV. The size of $I_{K,n}$ in +/*dn* IHCs was similar to that recorded from CD-1 mice (Marcotti *et al.* 2003*a*; Oliver *et al.* 2003).

Adult-type ionic currents from *Beethoven* mice are reduced in size

Since *deafness* and *Beethoven* are mutations of the same *Tmc1* gene, we investigated whether basolateral ion channels were also affected in hair cells from *Beethoven* mice. Earlier results had suggested that basolateral K^+ and Ca^{2+} currents developed normally in *Bth*/+ IHCs and OHCs up to P15 (Vreugde *et al.* 2002). Immature hair cells

from control (+/+) and mutant (*Bth*/+ and *Bth*/*Bth*) mice all had similar biophysical properties (data not shown), analogous to the results from immature *dn* mice. We also looked in immature *Bth* IHCs for the presence of the small-conductance Ca^{2+}-activated K^+ current (I_{SK}) which was previously demonstrated in immature CD-1 IHCs (Marcotti *et al.* 2004*b*). The current was evident as a slowly developing outward current (4 s voltage steps, as in Fig. 2*A* of Marcotti *et al.* 2004*b*) that was reversibly abolished in Ca^{2+}-free extracellular solution (*Bth*/*Bth*,

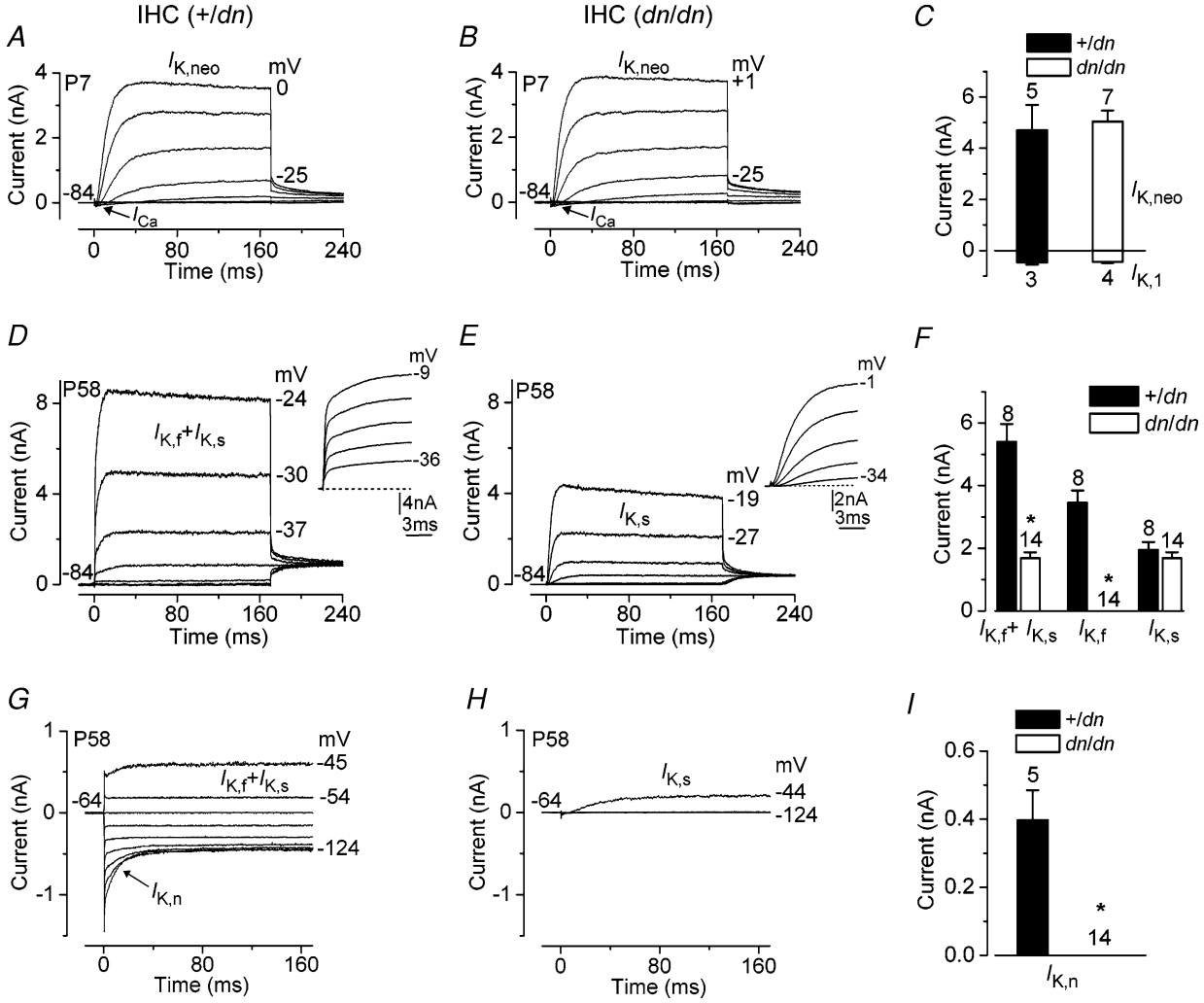

Figure 6. K^+ currents in IHCs from *deafness* mutant mice
A and *B*, current recordings under voltage clamp from control (+/*dn*) and mutant (*dn*/*dn*) immature apical-coil IHCs (P7), respectively. Outward K^+ currents ($I_{K,neo}$) were elicited in response to depolarizing voltage steps (10 mV nominal increments) from −104 mV starting from the holding potential of −84 mV. +/*dn*: V_m −72 mV; C_m 7.0 pF; R_s 1.7 MΩ; g_{leak} 4.0 nS; *dn*/*dn*: V_m −74 mV; C_m 8.3 pF; R_s 1.2 MΩ; g_{leak} 1.3 nS. Recordings were at room temperature. *C*, size of $I_{K,neo}$ and the inward rectifier K^+ current I_{K1} measured at 160 ms during voltage steps to 0 mV and −154 mV, respectively, in both +/*dn* and *dn*/*dn* IHCs. *D* and *E*, total outward K^+ currents recorded from +/*dn* ($I_{K,f} + I_{K,s}$) and *dn*/*dn* ($I_{K,s}$) apical IHCs (P58), respectively. Current recordings were elicited by applying depolarizing voltage steps in 10 mV nominal increments from −84 mV. The insets show the onset of the total current recorded from the same cells shown in *A* and *B* using shorter (20 ms) voltage steps of which the first 10 ms are shown. Note the slower current activation in *dn*/*dn* due to the absence of $I_{K,f}$. +/*dn*: V_m −72 mV; C_m 7.2 pF; R_s 1.3 MΩ; g_{leak} 12.0 nS. *dn*/*dn*: V_m −69 mV; C_m 6.4 pF; R_s 1.3 MΩ; g_{leak} 1.0 nS. *F*, size of the total steady-state currents ($I_{K,f} + I_{K,s}$) and the isolated $I_{K,f}$ and $I_{K,s}$ measured at −25 mV in both +/*dn* ($n = 8$, P18–P58) and *dn*/*dn* ($n = 14$, P17–P58) IHCs. *G* and *H*, membrane currents recorded from +/*dn* and *dn*/*dn* IHCs (P58) in response to voltage steps in 10 mV increments from −124 mV to more depolarized values starting from the holding potential of −64 mV. Note that $I_{K,f}$ and $I_{K,n}$ (as for OHCs) were not present in the mutant cell. +/*dn*: V_m −76 mV; C_m 9.1 pF; R_s 1.5 MΩ; g_{leak} 11.5 nS. *dn*/*dn*: V_m −64 mV; C_m 6.5 pF; R_s 1.9 MΩ; g_{leak} 0.4 nS. *I*, size of $I_{K,n}$ measured as the difference between instantaneous and steady-state deactivating tail currents for voltage steps from −64 mV to −124 mV in +/*dn* ($n = 5$, P41–P58) and *dn*/*dn* ($n = 14$, P41–P58) mice. Recordings in *D*–*I* were at body temperature.

P7, $n = 4$, data not shown). The apparently normal development of immature currents indicates that the mutations in *Tmc1* are unlikely to affect these cells before their onset of mature function (P8 for OHCs and P12 for IHCs).

Hair cells from mature *Bth* mutants did have abnormal expression of basolateral membrane currents. Figure 7*B*, *E* and *G* shows that the size of the total outward K^+ current from *Bth*/*Bth* IHCs and OHCs, recorded using voltage protocols similar to those described in Fig. 5 (for OHCs) and Fig. 6 (for IHCs), was considerably reduced when compared to that measured in controls (+/+, Fig. 7*A*, *D* and *F*, respectively). The average sizes of the total current ($I_{K,f} + I_{K,s}$) and the isolated $I_{K,f}$ and $I_{K,s}$ in control and

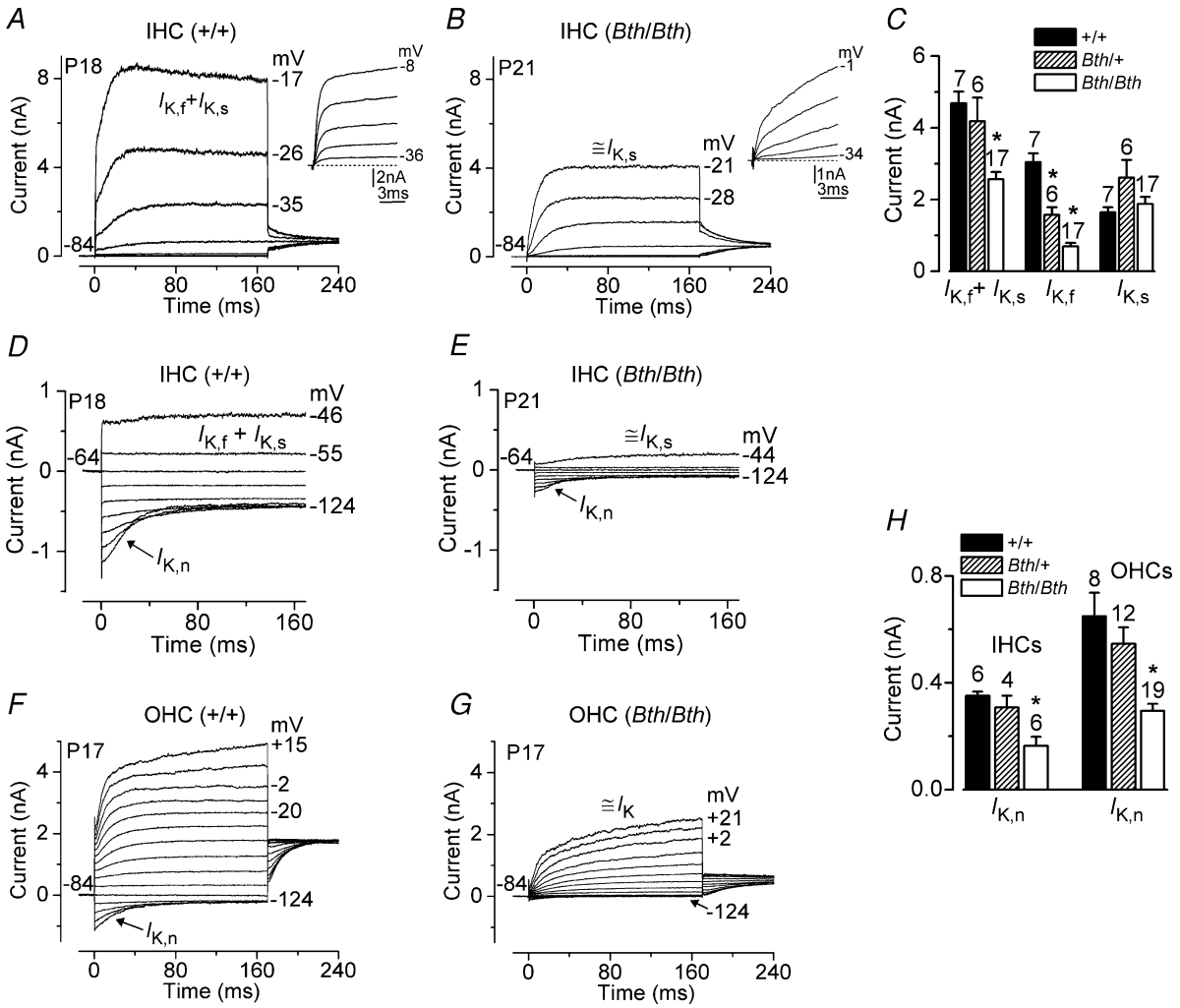

Figure 7. K^+ currents in mature IHCs and OHCs from *Beethoven* mutant mice
A and *B*, outward K^+ currents in a control IHC (+/+, P18) and a homozygous mutant IHC (*Bth*/*Bth*, P21), respectively. In this figure, all current recordings were obtained using the same voltage protocols described in Fig. 5 (for OHCs) and Fig. 6 (for IHCs). In contrast to *deafness* mutants, some residual $I_{K,f}$ is still present in the *Bth*/*Bth* IHC (*B*). +/+ IHC: V_m −75 mV; C_m 10.0 pF; R_s 0.4 MΩ; g_{leak} 6.0 nS. *Bth*/*Bth* IHC: V_m −76 mV; C_m 10.0 pF; R_s 1.6 MΩ; g_{leak} 2.0 nS. *C*, size of the total current ($I_{K,f} + I_{K,s}$) and the isolated $I_{K,f}$ and $I_{K,s}$ measured at −25 mV in +/+ ($n = 7$, P19–P20), *Bth*/+ ($n = 6$, P16–P22) and *Bth*/*Bth* ($n = 17$, P16–P22) IHCs. *D* and *E*, membrane currents recorded from P18 +/+ (*D*) and P21 *Bth*/*Bth* (*E*) IHCs. Note the small residual $I_{K,n}$ present in the *Bth*/*Bth* cell. Both cells are the same as in *A* and *B*. *F* and *G*, current recordings from +/+ (*F*) and *Bth*/*Bth* (*G*) P17 OHCs. As for IHCs, $I_{K,n}$ was very small in the *Bth*/*Bth* OHC. +/+ OHC: V_m −77 mV; C_m 10.8 pF; R_s 1.9 MΩ; g_{leak} 0.5 nS. *Bth*/*Bth* OHC: V_m −69 mV; C_m 10.0 pF; R_s 1.8 MΩ; g_{leak} 1.0 nS. *H*, size of $I_{K,n}$ measured as the difference between instantaneous and steady-state deactivating tail currents for voltage steps from −64 mV for IHCs and −84 mV for OHCs to −124 mV in +/+ (IHCs: $n = 6$, P41–P58; OHCs: $n = 8$, P15–P17), *Bth*/+ (IHCs: $n = 4$, P41–P58; OHCs: $n = 12$, P14–P17) and *Bth*/*Bth* (IHCs: $n = 7$, P41–P58; OHCs: $n = 19$, P14). The symbol ≅ before $I_{K,s}$ and I_K indicates that these currents are contaminated by residual currents not fully absent in *Bth*/*Bth* hair cells. All recordings were at room temperature.

mutant IHCs are shown in Fig. 7*C*. In contrast to *deafness* mice, $I_{K,f}$ was still present in *Beethoven* mutant IHCs, although its size was considerably reduced ($P < 0.0001$), more so in the homozygous mutants than in *Bth*/+. Post tests showed that $I_{K,f}$ of *Bth*/+ IHCs was both smaller than that of +/+ ($P < 0.001$) and larger than that of *Bth*/*Bth* ($P < 0.01$) IHCs. This corrects the earlier observation of normal development of basolateral currents in *Bth*/+ hair cells (Vreugde *et al.* 2002): the effect of the mutation on $I_{K,f}$ was probably missed because this current is still quite small just after the onset of hearing, and hair cell currents were only tested up to P15 in that study. Just as for *dn* mice, the size of $I_{K,s}$ did not seem to be affected by the mutation. In both cell types, $I_{K,n}$ could be observed in isolation during hyperpolarizing voltage steps as deactivating inward currents (Fig. 7*D* and *F*). It was again found to be reduced by the mutation in *Tmc1* (IHCs: $P < 0.0005$; OHCs: $P < 0.0001$), but only significantly so in *Bth*/*Bth* and not in *Bht*/+ (Fig. 7*H*).

We also investigated whether the ACh-activated current, which is normally expressed in adult OHCs (Evans, 1996; Dulon & Lenoir, 1996; He & Dallos, 1999) and in immature but not adult IHCs (Glowatzki & Fuchs, 2000; Katz *et al.* 2004; Marcotti *et al.* 2004*b*), was present in mutant cells. Currents were recorded from adult *Bth/Bth* hair cells during superfusion of 100 μM ACh as previously described (Marcotti *et al.* 2003*b*). As expected, the ACh-activated K^+ current, isolated by subtracting control currents from currents recorded in the presence of ACh, was expressed in OHCs (P20–P24, $n = 4$) but not in IHCs (P22, $n = 2$), so the ACh responses appeared qualitatively normal. The response of OHCs to ACh was quantified by measuring the steady-state slope conductance of the ACh-activated current around the holding potential of −84 mV (Marcotti *et al.* 2004*b*). The slope conductance in *Beethoven* mutant OHCs (*Bth*/*Bth*, 6.9 ± 0.7 nS, $n = 4$) was found to be significantly ($P < 0.05$) reduced compared to that measured in controls (+/+, 13.5 ± 2.1 nS, $n = 3$).

The exocytotic machinery in mutant IHCs remains at an immature stage of development

In normal CD-1 mice the size of I_{Ca} in IHCs increases from embryonic stages of development up to about P6, and then gradually decreases to a constant maximum size of about −100 pA (1.3 mM extracellular Ca^{2+} and at around −20 mV) after the onset of hearing (Marcotti *et al.* 2003*b*; Johnson *et al.* 2005). Although the size of I_{Ca} decreases during development, its activation kinetics are not significantly different between pre- and posthearing IHCs (Johnson *et al.* 2005). Moreover, the observation that the $Ca_{v1.3}$ Ca^{2+} channel subunit is responsible for >90% of I_{Ca} in immature as well as mature IHCs (Platzer *et al.* 2000; Brandt *et al.* 2003), indicates that the decline of the current starting at P6 is due to a reduction in the number of Ca^{2+} channels rather than a change in channel composition. Immature IHCs (P7) from both control and mutant *deafness* mice express an I_{Ca} of similar size to that previously reported for CD-1 mice of the same age (Marcotti *et al.* 2003*b*; Johnson *et al.* 2005). By contrast, I_{Ca} in mature IHCs was affected by the mutation. Figure 8*A* and *B* shows I_{Ca} recorded from P18 +/*dn* and *dn*/*dn* IHCs, respectively. The size of I_{Ca} recorded in mutant (both *dn* and *Bth*) IHCs was always larger than that found in controls (see Fig. 8*A*, *B* and *D* for *deafness*), but similar to that measured in immature, prehearing cells. The different inactivation kinetics between the control (+/*dn*) and mutant (*dn*/*dn*) IHCs shown in Fig. 8*A* and *B* are not due to the mutation but represent variations in the effectiveness of the block of contaminating outward K^+ currents seen also in IHCs from normal CD-1 mice (Johnson *et al.* 2005).

Because of the larger I_{Ca} size in mature mutant IHCs, we investigated whether exocytosis, a Ca^{2+}-dependent process that is considered to be a sign of neurotransmitter release from presynaptic cells (Parsons *et al.* 1994; Von Gersdorff *et al.* 1998; Moser & Beutner, 2000) was also affected. The degree of exocytosis, elicited by voltage steps, was estimated by measuring the change in cell membrane capacitance (ΔC_m). Figure 8*C* shows I_{Ca} and the corresponding ΔC_m recorded from mature +/*dn* (P17) and *dn*/*dn* (P18) IHCs using 100 ms voltage steps from −81 mV to near −21 mV, which elicited maximum I_{Ca}. Although the *dn*/*dn* IHC responded to the same voltage step with a significantly larger peak I_{Ca}, the size of the induced ΔC_m was similar to that seen in the +/*dn* cell. The peak I_{Ca}–voltage (I–V) and ΔC_m-voltage (ΔC_m–V) curves for +/*dn* ($n = 4$) and *dn*/*dn* ($n = 5$) cells were obtained from responses to 100 ms depolarizing voltage steps in nominal 10 mV increments from the holding potential of −81 mV (Fig. 8*D*). I_{Ca} and ΔC_m both followed a bell-shaped trend, but note the narrower voltage range for ΔC_m in homozygous mutant cells. The average peak size of I_{Ca} recorded in both *dn* and *Bth* mutants and controls is shown in Fig. 8*E*. I_{Ca} in homozygous mutant IHCs was significantly larger than that recorded in controls ($P < 0.05$) and normal age-matched CD-1 mice (*dn*/*dn*: $P < 0.001$; *Bth*/*Bth*: $P < 0.01$). The size of I_{Ca} in *Bth*/+ was intermediate, and did not differ significantly from that recorded in either +/+ or *Bth*/*Bth* IHCs, although it was larger ($P < 0.05$) than that in CD-1 IHCs. The average size of I_{Ca} in mature IHCs of homozygous *dn* and *Bth* mutants closely matches that recorded at about P6 in immature IHCs of normal CD-1 mice (Marcotti *et al.* 2003*b*; Johnson *et al.* 2005). The maximum ΔC_m was similar between all IHCs investigated, and also to that in adult CD-1 mice (Fig. 8*F*). In both mutant and control IHCs, ΔC_m for the largest I_{Ca} measured (at around −21 mV) was about 30 fF (femtofarad) implying that mature IHCs, whether mutant or not, were capable of releasing about 800 synaptic vesicles

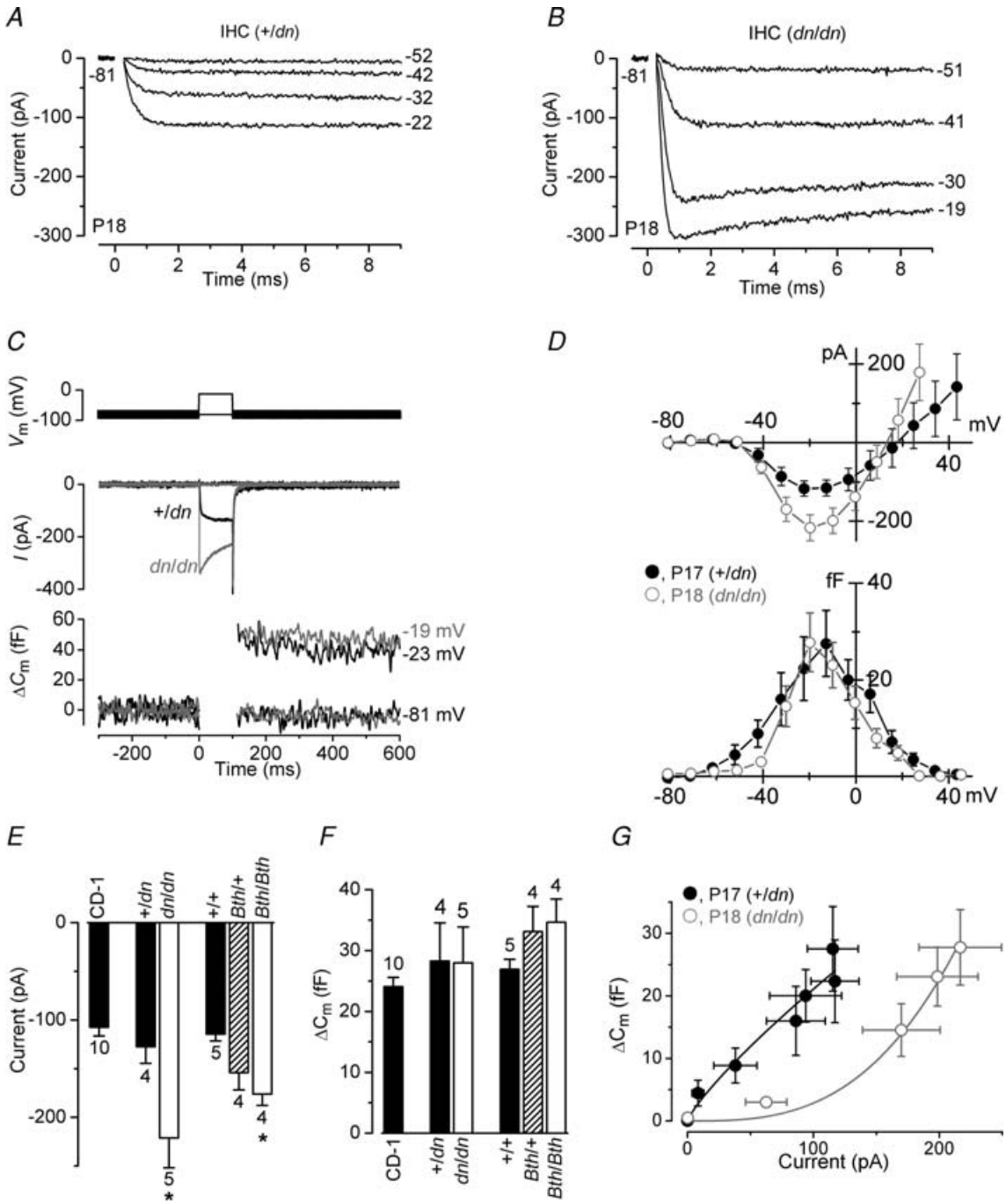

Figure 8. Ca^{2+} currents and ΔC_m in mature *deafness* and *Beethoven* IHCs
A and *B*, inward I_{Ca} recordings from +/*dn* and *dn*/*dn* IHCs (P18), respectively, in response to voltage steps from the holding potential of −81 mV to more depolarized levels in 10 mV increments. For clarity only some of the traces are shown and the membrane potentials (inmV) are indicated next to the traces. The current traces in *A* and *B* are averages from five and six repetitions, respectively. +/*dn*: C_m 8.3 pF; R_s 6.8 MΩ; g_{leak} 4.0 nS. *dn*/*dn*: C_m 6.3 pF; R_s 7.9 MΩ; g_{leak} 1.3 nS. *C*, I_{Ca} (middle panel) and ΔC_m (bottom panel) responses in adult IHCs from +/*dn* and *dn*/*dn* mice elicited by applying 100 ms depolarizing voltage steps from the holding potential of −81 mV to near −21 mV. +/*dn*: C_m 7.5 pF; R_s 6.0 MΩ; g_{leak} 3.2 nS; Peak I_{Ca} −145 pA elicited a ΔC_m of 45 fF. *dn*/*dn*: C_m 6.3 pF; R_s 7.9 MΩ; g_{leak} 0.4 nS; Peak I_{Ca} −336 pA elicited a ΔC_m of 49 fF. The command protocol (top panel) consists of a sinusoidal waveform (used to track C_m) that appears as a thick black line, which is interrupted for the duration of the voltage steps. *D*, peak current–voltage (I_{Ca}–V, upper panel) and capacitance–voltage (ΔC_m–V, lower panel) curves, measured at different membrane potentials from −81 mV to more depolarized potentials in nominal 10 mV increments, from the +/*dn* ($n = 4$, P17) and *dn*/*dn* ($n = 5$, P18) IHCs. *E*, average peak (near −21 mV) I_{Ca} recorded in mature IHCs from normal CD-1 (P16–P20), +/*dn* (P17), *dn*/*dn* (P18), +/+and *Bth*/+ (P16–P17) and *Bth*/*Bth* (P17).

in response to 100 ms voltage steps, using a conversion factor of 37 aF (attofarad) per vesicle (Lenzi *et al.* 1999). As their Ca^{2+} currents were larger, the Ca^{2+} efficiency of the mature mutant IHCs was thus reduced compared to normal mature IHCs (Johnson *et al.* 2005).

The relation between Ca^{2+} entry and exocytosis (Fig. 8*G*) for +/*dn* and *dn*/*dn* IHCs, estimated using a synaptic transfer function (Augustine *et al.* 1985; Johnson *et al.* 2005), was obtained by plotting ΔC_m against peak I_{Ca} for 100 ms voltage steps over the range from −81 mV to near −11 mV. Data were approximated using a power function:

$$\Delta C_m \propto I_{Ca}^N \quad (1)$$

where N is the power. The average power obtained from the transfer functions of mature +/*dn* IHCs was 0.82 ± 0.10 ($n = 4$), suggesting a near-linear relation between Ca^{2+} entry and exocytosis as previously described for mature IHCs from normal CD-1 mice (Johnson *et al.* 2005). The transfer curve obtained from *dn*/*dn* IHCs was best approximated using a power of 2.99 ± 0.46 ($n = 5$), significantly larger ($P < 0.005$) than that found in the controls, indicating that each release event requires around three Ca^{2+}-binding steps to occur (Dodge & Rahamimoff, 1967). The Ca^{2+} dependence of exocytosis in *Beethoven* IHCs was also significantly steeper than in control cells (*Bth*/*Bth*: 2.48 ± 0.38 $n = 3$; +/+: 0.72 ± 0.08 $n = 5$; $P < 0.05$, post test), with intermediate values for *Bth*/+ (1.36 ± 0.61 $n = 3$). This high-order dependence of exocytosis on Ca^{2+} entry and the lower Ca^{2+} efficiency in adult mutant IHCs is reminiscent of that found in prehearing IHCs of normal CD-1 mice (power $N \approx 3$, Johnson *et al.* 2005), suggesting that *Tmc1* is also likely to be involved in the maturation of the exocytotic machinery in these cells. Although the factors that lead to the developmental linearization in the Ca^{2+} dependence of exocytosis in normal IHCs are unknown, the expression of *Tmc1* might ensure the normal maturation (downregulation) of I_{Ca} and/or changes in the Ca^{2+}-sensing molecules of exocytosis from around the onset of hearing. These anomalies in exocytosis due to *Tmc1* mutations may reflect the apparently abnormal development or maintenance of synaptic connections previously reported in *deafness* mutant hair cells (Bock & Steel, 1983).

Voltage responses of IHCs under current clamp

Immature IHCs from normal CD-1 mice are capable of generating spontaneous or evoked repetitive Ca^{2+} action potentials prior to the onset of hearing (Kros *et al.* 1998; Glowatzki & Fuchs, 2000; Beutner & Moser, 2001; Marcotti *et al.* 2003*a*; Marcotti *et al.* 2003*b*). Figure 9*A* and *B* shows that immature P8 IHCs from both +/*dn* and *dn*/*dn* fire action potentials upon current injection. The same results were also obtained in both homo- and heterozygous *Beethoven* IHCs (P7). In the latter a Ca^{2+}-free extracellular solution was tested, which reversibly abolished the action potentials, demonstrating their Ca^{2+} dependence (data not shown). As in normal CD-1 mice, I_{Ca} expressed in heterozygous and homozygous *deafness* IHCs (see Fig. 6*A* and *B*, arrows) is likely to play the major role in the generation of action potentials. The mean resting membrane potential (V_m, mostly measured in current clamp but in some cases as zero-current potential) of immature IHCs was found not to be significantly different between control and mutant (*dn*/*dn*, *Bth*/+ and *Bth*/*Bth*) cells, and the values were pooled together (-74.1 ± 0.8 mV, $n = 29$, P6–P8). The same applied to the V_m of control and mutant immature OHCs (-67.2 ± 1.2 mV, $n = 15$, P6–P8). Since the disappearance of induced action potentials in IHCs at the onset of hearing was previously correlated with the expression of $I_{K,f}$ (Kros *et al.* 1998) and $I_{K,n}$ (Marcotti *et al.* 2003*a*), we investigated how the absence of these currents affected the voltage responses of adult mutant cells. In +/*dn* IHCs, small hyperpolarizing and depolarizing current injections produced fast, small and graded voltage responses (Fig. 9*C*) as previously described in IHCs of normal CD-1 mice (Kros *et al.* 1998; Marcotti *et al.* 2004*a*). In adult *dn*/*dn* IHCs, small hyperpolarizing current injections caused large and almost passive voltage responses (Fig. 9*D*), most likely due to the absence of both $I_{K,n}$ and $I_{K,f}$, which in normal hair cells are both partially active around the resting membrane potential (Marcotti *et al.* 2003*a*, 2004*a*; Oliver *et al.* 2003). Voltage changes in response to depolarizing current injections were always much larger but slower in onset than in *dn*/*dn* IHCs (Fig. 9*D*) compared to those recorded from +/*dn* cells (Fig. 9*C*). Moreover, small depolarizing current injections generated slow oscillatory responses reminiscent of the small action potentials recorded from late embryonic IHCs (Marcotti *et al.* 2003*a*,*b*). Voltage oscillations were never observed in mature *Bth*/+ and *Bth*/*Bth* IHCs, but voltage responses to depolarizing and hyperpolarizing current steps appeared larger and slower than in controls, particularly in *Bth*/*Bth* IHCs. These voltage responses were not analysed in detail but resembled those observed when TEA was used to block $I_{K,f}$ (Kros & Crawford, 1990) or BAPTA to shift its operating range in the

F, average ΔC_m measured in response to the I_{Ca} recorded in *E*. *G*, average ΔC_m responses plotted against the corresponding I_{Ca} size from the *I*–*V* and ΔC_m–*V* curves shown in (*D*). Continuous lines are fits to data points according to eqn 1. All recordings were at body temperature.

depolarizing direction (Marcotti *et al.* 2004*a*). Figure 9*E* and *F* shows the resting membrane potential (V_m) in adult IHCs (Fig. 9*E*) and OHCs (Fig. 9*F*) from mutants and controls. In homozygous mutant hair cells, V_m was found to be significantly depolarized (IHCs: *dn*/*dn* $P < 0.0001$; *Bth*/*Bth* $P < 0.05$; OHCs: *dn*/*dn* $P < 0.005$; *Bth*/*Bth* $P < 0.001$) relative to that measured in control cells from the same strains. In *Bth*/+, V_m was similar to the controls and more hyperpolarized than *Bth*/*Bth* in both cell types ($P < 0.01$).

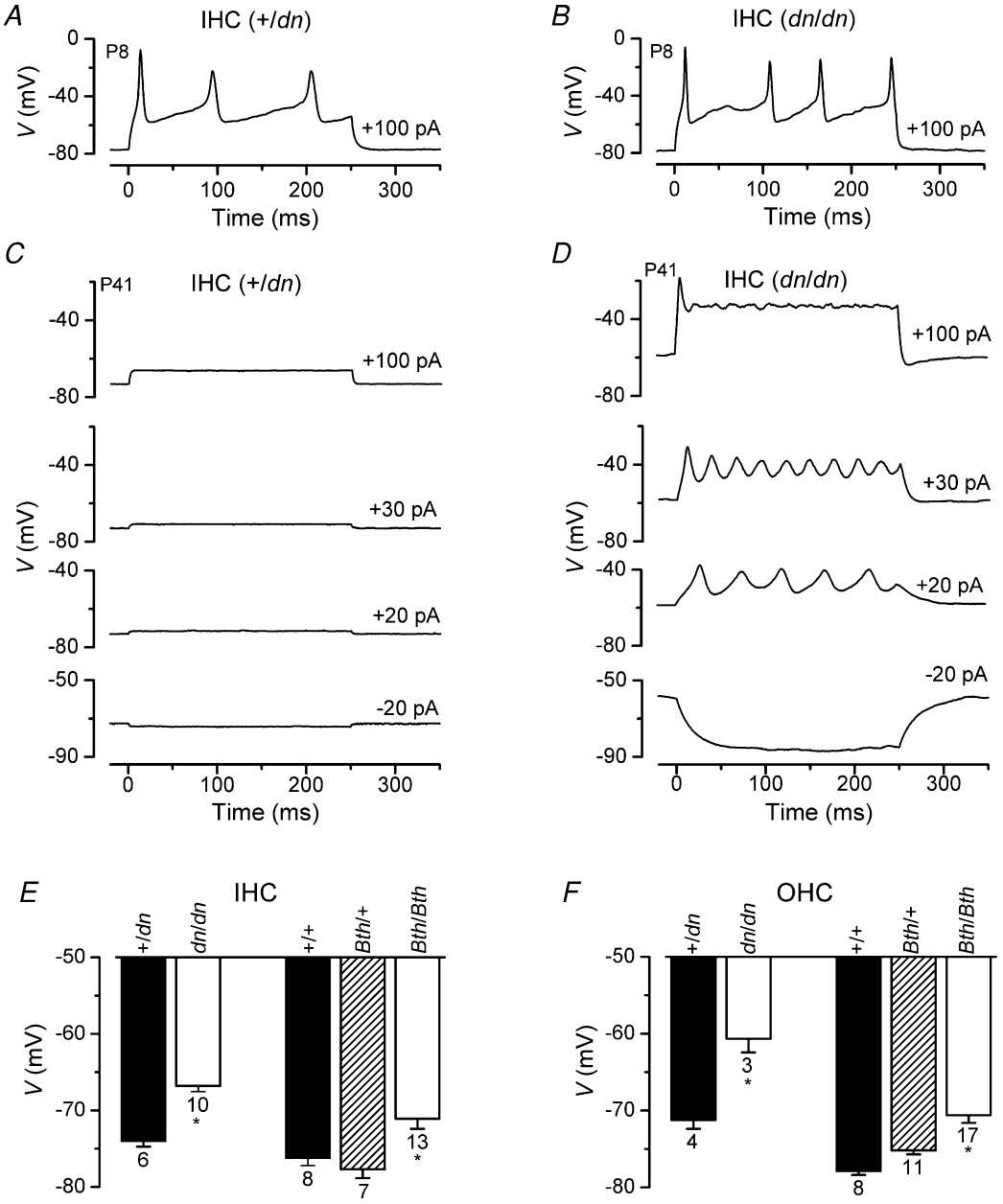

Figure 9. Voltage responses of IHCs from *deafness* mice
A and *B*, voltage responses under current clamp from +/*dn* (*A*) and *dn*/*dn* (*B*) IHCs at P8. Depolarizing current injections (+100 pA) triggered action potentials. The membrane potential (*V*) is plotted along the ordinates. +/*dn*: V_m −78 mV; C_m 9.4 pF; R_s 5.0 MΩ. *dn*/*dn*: V_m −79 mV; C_m 9.9 pF; R_s 6.2 MΩ. *C*, voltage responses from a P41 +/*dn* IHC. V_m −74 mV; C_m 8.2 pF; R_s 7.1 MΩ. *D*, voltage responses from a P41 *dn*/*dn* IHC exhibiting slow repetitive action potentials when small current injections were applied. V_m −64 mV; C_m 6.2 pF; R_s 6.2 MΩ. *E* and *F*, average resting membrane potentials (V_m) of IHCs and OHCs, respectively, from *dn* and *Bth* mutant mice. IHCs: +/*dn*, P18–P58; *dn*/*dn*, P17–P58; +/+, *Bth*/+ and *Bth*/*Bth*, P19–P20. OHCs: +/*dn* and *dn*/*dn*, P14; +/+ and *Bth*/+, P14–P17; *Bth*/*Bth*, P12–P17. All recordings were at body temperature.

Discussion

Both the *dn* and *Bth* mutations in mouse and the DFNA36 and DFNB7/B11 loci in humans lead to hearing impairment by affecting the *Tmc1* (*TMC1*) gene (Vreugde *et al.* 2002; Kurima *et al.* 2002). Although the function of *Tmc1* is unknown, its expression in both IHCs and OHCs in early postnatal development (from P5: Kurima *et al.* 2002; Vreugde *et al.* 2002) suggests that it might play a role in the normal maturation of these cells. Therefore, in the present study we examined the effects that mutations in *Tmc1* have on the structural appearance and biophysical properties of immature and mature cochlear hair cells using the *deafness* and *Beethoven* mouse mutants.

Mutations in *Tmc1* can impede the development of cochlear hair cells into fully functional sensory receptors

After terminal mitosis, at about embryonic day 14–15 in normal mice (Pujol *et al.* 1998), hair cell precursors start to differentiate electrophysiologically by acquiring a small delayed-rectifier K^+ current (Marcotti *et al.* 2003*a*; Helyer *et al.* 2005). During the following two weeks, hair cells undergo extensive biophysical changes mainly due to the acquisition of the mechano-electrical transducer current and various basolateral membrane currents (Fig. 10*A* and *B*). Immature IHCs generate trains of spontaneous action potentials (Kros *et al.* 1998; Marcotti *et al.* 2003*a*, 2003*b*)

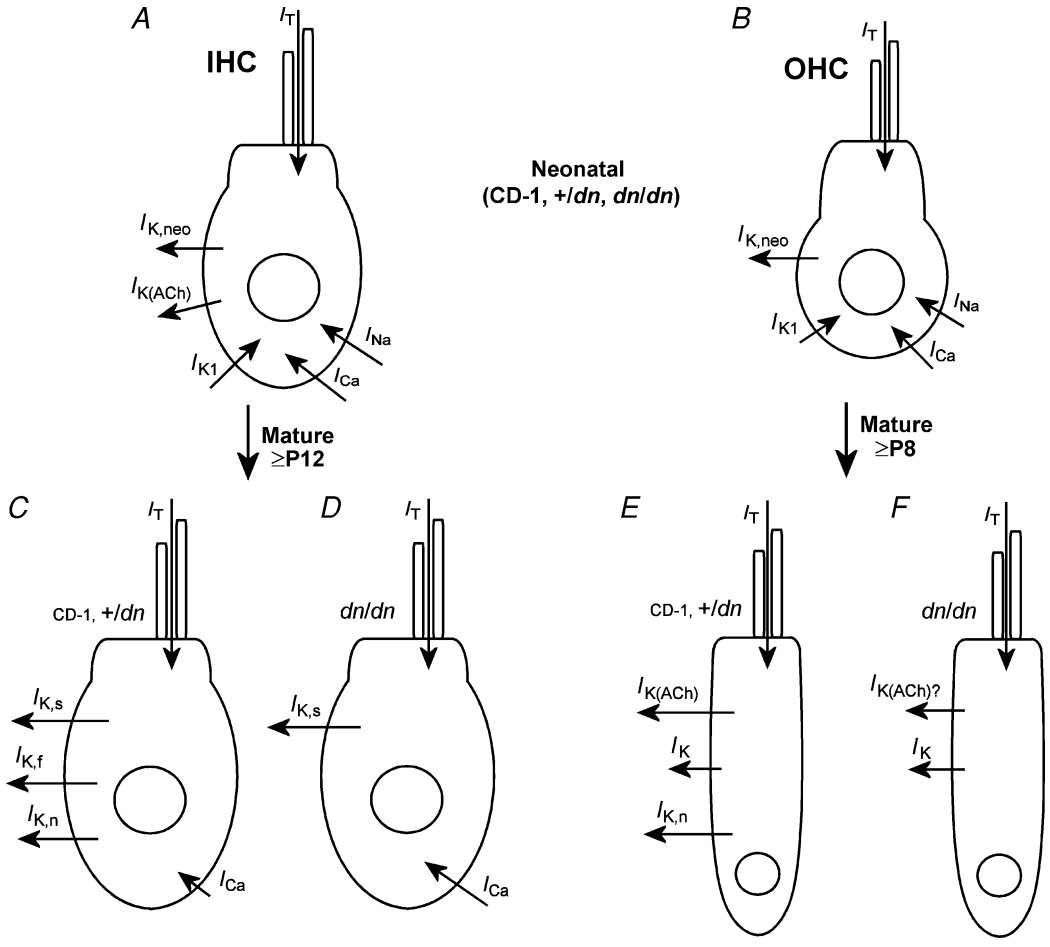

Figure 10. Main physiological differences between immature and mature hair cells from normal CD-1 mice and *deafness* mutant mice

A and *B*, schematic representation showing the different types of membrane currents likely to be expressed in immature IHCs (*A*) and OHCs (*B*) from normal CD-1 , +/*dn* and *dn*/*dn* mice. *C* and *E*, currents expressed by mature hair cells of +/*dn* and normal CD-1 mice. *D* and *F*, membrane currents expressed in mutant hair cells. For $I_{K(ACh)}$ there is some uncertainty as the data are only from *Bth*/*Bth*. I_T is the mechano-electrical transducer current. The effects of the *Tmc1* mutation on the various ionic currents are qualitatively similar but less severe in *Bth*/*Bth* and least severe in *Bth*/+ (see text for details).

prior to the onset of sound-induced responses, thought to be involved in the refinement of synaptic connections within the immature cochlea by analogy with the visual system (Zhang & Poo, 2001). With the onset of functional maturation at P8 in OHCs (Marcotti & Kros, 1999) and P12 in IHCs (Kros *et al.* 1998; Marcotti *et al.* 2003*a*), most of the basolateral membrane currents expressed in immature hair cells are partially or completely down-regulated (IHC: Fig. 10*A* and *C*; OHC: Fig. 10*B* and *E*). At the same time the acquisition of $I_{K,f}$ and $I_{K,n}$ in IHCs and $I_{K,n}$, $I_{K,(ACh)}$ and electromotility in OHCs (Figs 10*C* and *E*) changes these cells into fully functional sensory receptors.

Single-cell recordings from *dn*/*dn*, *Bth*/+ and *Bth*/*Bth* mice show that immature hair cells express basolateral membrane and mechano-electrical transducer currents that are indistinguishable from those found in controls or normal CD-1 mice, suggesting that prehearing cells are unlikely to be affected by mutations in *Tmc1*. The development of normal transducer currents in the mutant OHCs shows that *Tmc1* does not encode a component of the transducer channel, and makes it likely that the inability to record cochlear microphonics from *dn*/*dn* mice is simply a consequence of the degeneration of large numbers of OHCs. The most striking effect of *Tmc1* mutations is the absence (*dn*/*dn*) or the reduced (*Bth*/*Bth* and, to a more modest extent, *Bth*/+) expression of K^+ currents that characterize the mature hair cell phenotype (Fig. 10*D* and *F*). Moreover, the size of I_{Ca} in mutant adult IHCs (*dn*/*dn*, *Bth*/+ and *Bth*/*Bth*) is larger than that recorded in age-matched control (+/*dn* and, for *Bth*, +/+) cells, but similar to that measured in immature IHCs from both controls and mutants (see Results for *deafness*) and normal CD-1 mice (Beutner & Moser, 2001; Marcotti *et al.* 2004*b*; Johnson *et al.* 2005), indicating that its normal maturation has also been altered. It is thus likely that *Tmc1* mutations prevent the apparently normal downregulation of the Ca^{2+} current starting in the second postnatal week (Beutner & Moser, 2001; Marcotti *et al.* 2003*b*). Despite this large I_{Ca}, maximum Ca^{2+}-induced exocytosis was similar between controls and mutant adult IHCs, indicative of a reduced Ca^{2+} efficiency in the mutants. Moreover, the Ca^{2+} dependence of exocytosis was steeper in mutant cells. Since a high-order Ca^{2+} dependence of exocytosis has only been found in prehearing IHCs (Johnson *et al.* 2005), it seems conceivable that *Tmc1* also plays a role in the normal maturation of the exocytotic machinery. However, the presence of electromotile activity in adult mutant OHCs, and their responsiveness to ACh, together with the normal developmental downregulation of most of the immature-type currents in both cell types suggest that mutations in *Tmc1* do not cause a general failure of hair cell maturation, but instead prevent the acquisition of specific adult phenotypes.

Physiological consequences of mutations in *Tmc1* in the organ of Corti

Scanning electron microscopy of *dn*/*dn* and *Bth*/*Bth* mutants revealed progressive hair cell degeneration from P15 onwards. This degeneration is unlikely to be the direct cause for the raised thresholds for CAP responses (*dn*/*dn*: Bock & Steel, 1983; *Bth*/*Bth*: Fig. 3*A* and *B*), because many hair cells remain with hair bundles of normal appearance, especially in the apex (80–90% region, Figs 1 and 2 and Vreugde *et al.* 2002). The presence of apparently healthy apical cells could conceivably be explained by assuming that the expression of *Tmc1* was restricted to the middle and basal regions of the cochlea, as recently shown for the chick basilar papilla (Mutai *et al.* 2005), the avian equivalent of the organ of Corti. However, our electrophysiological findings show that apical hair cell function is directly affected by the mutation, indicating that the electrically resonant low-frequency region of the basilar papilla may be a special case that is different from the mammalian cochlea and one in which *Tmc1 has* no functional role.

In mammals, the hearing impairment associated with *Tmc1* mutations is most likely due to the absence (in *dn*) or reduced expression (in *Bth*) of adult-type currents, and the lack of maturation of the exocytotic machinery. $I_{K,n}$ is substantially (about 70%) activated at the resting membrane potentials of adult OHCs (Marcotti & Kros, 1999) and IHCs (Marcotti *et al.* 2003*a*; Oliver *et al.* 2003), providing an efficient exit route for K^+ ions entering the cells through the transducer channels. In IHCs this role is aided by $I_{K,f}$, since it contributes about half of the resting conductance (Marcotti *et al.* 2004*a*). The absence of $I_{K,n}$ in mutant OHCs and of both $I_{K,n}$ and $I_{K,f}$ in IHCs might lead to an accumulation of intracellular K^+ that could be responsible for the progressive degeneration of these cells observed in mutant mice. The slower progression of hair cell degeneration in the apex could be due to the smaller transducer currents in this region (He *et al.* 2004). Slow degeneration of hair cells has been inferred for DFNA2, another form of non-syndromic dominant progressive hearing loss in humans starting at high frequencies, caused by mutation of the *KCNQ4* gene (Kubisch *et al.* 1999; Kharkovets *et al.* 2006) that is likely to underlie $I_{K,n}$ in hair cells (Marcotti & Kros, 1999; Marcotti *et al.* 2003*a*; Oliver *et al.* 2003). The absence of $I_{K,f}$ in *dn*/*dn* IHCs, which is believed to be essential for high-frequency phase locking in the auditory nerve (Palmer & Russell, 1986; Kros & Crawford, 1990), allows these cells to fire slow Ca^{2+} action potentials even at adult stages (up to P58, the oldest stage investigated). These action potentials (Fig. 9*D*), together with the steeper Ca^{2+} dependence of exocytosis (Fig. 8*G*), which results in a more depolarized threshold for neurotransmitter release, would prevent adult IHCs of *dn*/*dn* from accurately encoding high-frequency sound stimuli (Johnson *et al.* 2005). Synchronous neural activity is

required for generation of a CAP, so abnormal action potentials in mature mutant IHCs could lead to the absence of the CAPs in *dn*/*dn* (Bock & Steel, 1983) The absence of normal auditory nerve activity of cochlear origin has been suggested as the possible cause of the increased transmitter release probability (Oleskevich & Walmsley, 2002), altered inhibitory transmission (Leao *et al.* 2004*a*) and enhanced cell excitability (Leao *et al.* 2004*b*) observed in auditory brain stem neurons of *dn*/*dn* mutants studied *in vitro*. Action potentials were not observed in *Bth*/*Bth* IHCs, but their voltage responses were slower and larger than normal. Together with the more depolarized threshold for neurotransmitter release, this could partially but perhaps not fully explain the absence of CAP responses in *Bth*/*Bth* mice. In mature *Bth*/+ cochlear hair cells, the various K^+ currents were only somewhat smaller than the controls, and the Ca^{2+} current was somewhat larger, but with the exception of $I_{K,f}$ in IHCs not significantly so. Exocytosis also appeared nearly normal. Perhaps with more experiments, statistical significance might have been achieved. It seems likely that because of these near-normal properties reasonable CAP responses could be recorded from *Bth*/+ mice over the full frequency range by P15, with the later deterioration at high frequencies at P30 and P60 following the progress of hair cell degeneration due to impaired K^+ efflux from the basolateral membrane. Finally, the more depolarized membrane potential observed in homozygous mutant IHCs, due to the partial (*Bth*/*Bth*) or complete (*dn*/*dn*) absence of $I_{K,n}$ and $I_{K,f}$ (Figs 5–7), would of itself increase resting I_{Ca} in mature mutant IHCs, which could raise the intracellular Ca^{2+} levels (Oliver *et al.* 2003), possibly leading to cytotoxicity and cell degeneration (Orrenius *et al.* 2003).

Possible functional roles of Tmc1

Tmc1 encodes a transmembrane protein predicted to have 6–11 transmembrane domains with charged intracellular amino and carboxy termini (Kurima *et al.* 2002; Vreugde *et al.* 2002), reminiscent of voltage-gated channels (Hille, 2001). Our finding of relatively modest defects in hair cell physiology and slower degeneration of the organ of Corti in *Bth*/+ than in *Bth*/*Bth* mice, together with the absence of any obvious defects in +/*dn* mice, suggests that the *Bth* allele acts through a dominant negative mechanism rather than through haploinsufficiency, while the *dn* allele is likely to be a functional null mutation. This is compatible with the notion that the Tmc1 protein may be a multimer of which the function is disturbed by the incorporation of *Bth* subunits. Tmc1 protein appears to be localized in the area surrounding the hair cell cuticular plate and at the endoplasmic reticulum from P10 (Makishima *et al.* 2005). The presence of TMC1 in endoplasmic reticulum membrane was also demonstrated in Cos7 cells (Labay *et al.* 2005). *Tmc1* is unlikely to encode an ion channel since when mutated it appears to interfere with the normal development of a number of different ion channel types ($I_{K,f}$, $I_{K,n}$, I_{Ca} and possibly $I_{K(ACh)}$). Moreover, such mutations also prevent the maturation of the synaptic machinery. However, *Tmc1* could be responsible for up- or downregulating various ion channels or exocytotic molecules during development.

Channel expression can be regulated by Ca^{2+} entry into the cell (Linsdell & Moody, 1995; Liu & Kaczmarek, 1998*a*; Muller *et al.* 1998; Xie & Black, 2001) and/or by neurotrophic factors via the activation of intracellular signalling pathways (Liu & Kaczmarek, 1998*b*; Dryer *et al.* 2003; Huang & Reichardt, 2003). In mature cochlear IHCs from mice lacking the $Ca_v1.3$ L-type Ca^{2+} channel, which contributes 90% of the total Ca^{2+} current in these cells (Platzer *et al.* 2000), $I_{K,f}$ is absent (Brandt *et al.* 2003), suggesting that I_{Ca} is necessary for the appearance of $I_{K,f}$. The absence or reduced expression of $I_{K,f}$ in IHCs with *Tmc1* mutations is not due to the lack of I_{Ca}, since the latter is in fact unusually large in these cells. The possibility that mutations in *Tmc1* only cause a delay in the normal physiological maturation of cochlear hair cells, as previously described for mice lacking thyroid hormone receptors (Rüsch *et al.* 1998, 2001), where the maturation of $I_{K,f}$ was delayed by about two weeks, was considered. Transmission electron microscopy has shown that the opening of the spaces of Nuel around the OHCs of homozygous *deafness* mice was delayed by about 10 days (Bock & Steel, 1983). This delay may well be a consequence of the finding presented here that $I_{K,n}$ never develops in *dn*/*dn* OHCs, hampering the K^+ recycling pathway at this point (Steel & Kros, 2001). However, a general delay in hair cell maturation is unlikely as an explanation for our observations, since the effects of the *Tmc1* mutations were still evident in IHCs from two-month-old *dn*/*dn* mice.

Tmc1 expression could be involved in the activation or modulation of intracellular signals responsible for the physiological differentiation of immature hair cells into fully functional sensory receptors. Alternatively, *Tmc1* could be involved in intracellular trafficking, such as controlling the exit of various membrane proteins characteristic of mature hair cells from the endoplasmic reticulum (Ellgaard & Helenius, 2003; Vandenberghe & Bredt, 2004) before being inserted into the plasma membrane.

References

Augustine GJ, Charlton MP & Smith SJ (1985). Calcium entry and transmitter release at voltage-clamped nerve terminals of squid. *J Physiol* **367**, 163–181.

Beutner D & Moser T (2001). The presynaptic function of mouse cochlear inner hair cells during development of hearing. *J Neurosci* **21**, 4593–4599.

Bock GR, Frank MP & Steel KP (1982). Preservation of central auditory function in the deafness mouse. *Brain Res* **239**, 608–612.

Bock GR & Steel KP (1983). Inner ear pathology in the deafness mutant mouse. *Acta Otolaryngol* **96**, 39–47.

Brandt A, Striessnig J & Moser T (2003). $Ca_V1.3$ channels are essential for development and presynaptic activity of cochlear inner hair cells. *J Neurosci* **23**, 10832–10840.

Crawford AC, Evans MG & Fettiplace R (1989). Activation and adaptation of transducer currents in turtle hair cells. *J Physiol* **419**, 405–434.

Dallos P, Billone MC, Durrant JD, Wang C & Raynor S (1972). Cochlear inner and outer hair cells: functional differences. *Science* **177**, 356–358.

Dodge FA & Rahamimoff R (1967). Co-operative action of calcium ions in transmitter release at the muscular junction. *J Physiol* **193**, 419–432.

Dryer SE, Lhuillier L, Cameron JS & Martin-Caraballo M (2003). Expression of K(Ca) channels in identified populations of developing vertebrate neurons: role of neurotrophic factors and activity. *J Physiol* **97**, 49–58.

Dulon D & Lenoir M (1996). Cholinergic responses in developing outer hair cells of the rat cochlea. *Eur J Neurosci* **8**, 1945–1952.

Durham D, Rubel EW & Steel KP (1989). Cochlear ablation in deafness mutant mice: 2-deoxyglucose analysis suggests no spontaneous activity of cochlear origin. *Hear Res* **43**, 39–46.

Eatock RA & Hurley KM (2003). Functional development of hair cells. *Curr Topics Dev Biol* **57**, 389–448.

Ehret G (1975). Masked auditory thresholds, critical ratios, and scales of the basilar membrane of the housemouse (*Mus musculus*). *J Comp Physiol* **103**, 329–341.

Ellgaard L & Helenius A (2003). Quality control in the endoplasmic reticulum. *Nat Rev Mol Cell Biol* **4**, 181–191.

Evans MG (1996). Acetylcholine activates two currents in guinea-pig outer hair cells. *J Physiol* **491**, 563–578.

Géléoc GSG, Lennan GWT, Richardson GP & Kros CJ (1997). A quantitative comparison of mechanoelectrical transduction in vestibular and auditory hair cells of neonatal mice. *Proc R Soc Lond B* **264**, 611–621.

Glowatzki E & Fuchs PA (2000). Cholinergic synaptic inhibition of inner hair cells in the neonatal mammalian cochlea. *Science* **288**, 2366–2368.

He DZ & Dallos P (1999). Development of acetylcholine-induced responses in neonatal gerbil outer hair cells. *J Neurophysiol* **81**, 1162–1170.

He DZ, Evans BN & Dallos P (1994). First appearance and development of electromotility in neonatal gerbil outer hair cells. *Hear Res* **78**, 77–90.

He DZ, Jia S & Dallos P (2004). Mechanoelectrical transduction of adult outer hair cells studied in a gerbil hemicochlea. *Nature* **429**, 766–770.

Helyer RJ, Kennedy HJ, Davies D, Holley MC & Kros CJ (2005). Development of outward potassium currents in inner and outer hair cells from the embryonic mouse cochlea. *Audiol Neurootol* **10**, 22–34.

Hille B (2001). *Ion Channels of Excitable Membranes*, 3rd edn. Sinauer Associates, Sunderland, MA.

Hrabé de Angelis MH, Flaswinkel H, Fuchs H, Rathkolb B, Soewarto D, Marschall S, Heffner S, Pargent W, Wuensch K, Jung M, Reis A, Richter T, Alessandrini F, Jakob T, Fuchs E, Kolb H, Kremmer E, Schaeble K, Rollinski B, Roscher A, Peters C, Meitinger T, Strom T, Steckler T, Holsboer F, Klopstock T, Gekeler F, Schindewolf C, Jung T, Avraham K, Behrendt H, Ring J, Zimmer A, Schughart K, Pfeffer K, Wolf E & Balling R (2000). Genome-wide, large-scale production of mutant mice by ENU mutagenesis. *Nat Genet* **25**, 444–447.

Huang EJ & Reichardt LF (2003). Trk receptors: roles in neuronal signal transduction. *Annu Rev Biochem* **72**, 609–642.

Hunter-Duvar IM (1978). A technique for preparation of cochlear specimens for assessment with the scanning electron microscope. *Acta Otolaryngol Suppl* **351**, 3–23.

Johnson SL, Marcotti W & Kros CJ (2005). Increase in efficiency and reduction in Ca^{2+} dependence of exocytosis during development of mouse inner hair cells. *J Physiol* **563**, 177–191.

Johnson SL, Thomas MV & Kros CJ (2002). Membrane capacitance measurement using patch clamp with integrated self-balancing lock-in amplifier. *Pflugers Arch* **443**, 653–663.

Katz E, Elgoyhen AB, Gomez-Casati ME, Knipper M, Vetter DE, Fuchs PA & Glowatzki E (2004). Developmental regulation of nicotinic synapses on cochlear inner hair cells. *J Neurosci* **24**, 7814–7820.

Kharkovets T, Dedek K, Maier H, Schweizer M, Khimich D, Nouvian R, Vardanyan V, Leuwer R, Moser T & Jentsch TJ (2006). Mice with altered KCNQ4 K^+ channels implicate sensory outer hair cells in human progressive deafness. *EMBO J* **25**, 642–652.

Kros CJ & Crawford AC (1990). Potassium currents in inner hair cells isolated from the guinea-pig cochlea. *J Physiol* **421**, 263–291.

Kros CJ, Ruppersberg JP & Rüsch A (1998). Expression of a potassium current in inner hair cells during development of hearing in mice. *Nature* **394**, 281–284.

Kros CJ, Rüsch A & Richardson GP (1992). Mechano-electrical transducer currents in hair cells of the cultured neonatal mouse cochlea. *Proc R Soc Lond B* **249**, 185–193.

Kubisch C, Schroeder BC, Friedrich T, Lütjohann B, El-Amraoui A, Marlin S, Petit C & Jentsch TJ (1999). KCNQ4, a novel potassium channel expressed in sensory outer hair cells, is mutated in dominant deafness. *Cell* **96**, 437–446.

Kurima K, Peters LM, Yang Y, Riazuddin S, Ahmed ZM, Naz S, Arnaud D, Drury S, Mo J, Makishima T, Ghosh M, Menon PS, Deshmukh D, Oddoux C, Ostrer H, Khan S, Riazuddin S, Deininger PL, Hampton LL, Sullivan SL, Battey JF Jr, Keats BJ, Wilcox ER, Friedman TB & Griffith AJ (2002). Dominant and recessive deafness caused by mutations of a novel gene, *TMC1*, required for cochlear hair-cell function. *Nat Genet* **30**, 277–284.

Labay V, Makishima T & Griffith A (2005). Transmembrane topologic organization of TMC1. *Assoc Res Otolaryngol Abstract* 795.

Leao RN, Berntson A, Forsythe ID & Walmsley B (2004*b*). Reduced low-voltage activated K^+ conductances and enhanced central excitability in a congenitally deaf (*dn/dn*) mouse. *J Physiol* **559**, 25–33.

Leao RN, Oleskevich S, Sun H, Bautista M, Fyffe RE & Walmsley B (2004*a*). Differences in glycinergic mIPSCs in the auditory brain stem of normal and congenitally deaf neonatal mice. *J Neurophysiol* **91**, 1006–1012.

Lenzi D, Runyeon JW, Crum J, Ellisman MH & Roberts WM (1999). Synaptic vesicle populations in saccular hair cells reconstructed by electron tomography. *J Neurosci* **19**, 119–132.

Linsdell P & Moody WJ (1995). Electrical activity and calcium influx regulate ion channel development in embryonic *Xenopus* skeletal muscle. *J Neurosci* **15**, 4507–4514.

Liu SQ & Kaczmarek LK (1998*a*). The expression of two splice variants of the Kv3.1 potassium channel gene is regulated by different signaling pathways. *J Neurosci* **18**, 2881–2890.

Liu SQ & Kaczmarek LK (1998*b*). Depolarization selectively increases the expression of the Kv3.1 potassium channel in developing inferior colliculus neurons. *J Neurosci* **18**, 8758–8769.

Makishima T, Macnamare R, Kurima K & Griffith A (2005). Expression and localization studies of the TMC1 protein. *Assoc Res Otolaryngol Abstract* 625.

Marcotti W, Géléoc GSG, Lennan GWT & Kros CJ (1999). Developmental expression of an inwardly rectifying potassium conductance in inner and outer hair cells along the mouse cochlea. *Pflugers Arch* **439**, 113–122.

Marcotti W, Johnson SL, Holley MC & Kros CJ (2003*a*). Developmental changes in the expression of potassium currents of embryonic, neonatal and mature mouse inner hair cells. *J Physiol* **548**, 383–400.

Marcotti W, Johnson SL & Kros CJ (2004*a*). Effects of intracellular stores and extracellular Ca^{2+} on Ca^{2+}-activated K^+ currents in mature mouse inner hair cells. *J Physiol* **557**, 613–633.

Marcotti W, Johnson SL & Kros CJ (2004*b*). A transiently expressed SK current sustains and modulates action potential activity in immature mouse inner hair cells. *J Physiol* **560**, 691–708.

Marcotti W, Johnson SL, Rüsch A & Kros CJ (2003*b*). Sodium and calcium currents shape action potentials in immature mouse inner hair cells. *J Physiol* **552**, 743–761.

Marcotti W & Kros CJ (1999). Developmental expression of the potassium current $I_{K,N}$ contributes to maturation of the mouse outer hair cells. *J Physiol* **520**, 653–660.

Marcotti W, van Netten SM & Kros CJ (2005). The aminoglycoside antibiotic dihydrostreptomycin rapidly enters hair cells through the mechano-electrical transducer channel. *J Physiol* **567**, 505–521.

Moser T & Beutner D (2000). Kinetics of exocytosis and endocytosis at the cochlear inner hair cell afferent synapse of the mouse. *Proc Natl Acad Sci U S A* **97**, 883–888.

Muller YL, Reitstetter R & Yool AJ (1998). Regulation of Ca^{2+}-dependent K^+ channel expression in rat cerebellum during postnatal development. *J Neurosci* **18**, 16–25.

Mutai H, Mann S & Heller S (2005). Identification of chicken transmembrane channel-like (*TMC*) genes: expression analysis in the cochlea. *Neurosci* **132**, 1115–1122.

Ohmori H (1985). Mechano-electrical transduction currents in isolated vestibular hair cells of the chick. *J Physiol* **359**, 189–217.

Oleskevich S & Walmsley B (2002). Synaptic transmission in the auditory brainstem of normal and congenitally deaf mice. *J Physiol* **540**, 447–455.

Oliver D, Knipper M, Derst C & Fakler B (2003). Resting potential and submembrane calcium concentration of inner hair cells in the isolated mouse cochlea are set by KCNQ-type potassium channels. *J Neurosci* **23**, 2141–2149.

Orrenius S, Zhivotovsky B & Nicotera P (2003). Regulation of cell death: the calcium-apoptosis link. *Nat Rev Mol Cell Biol* **4**, 552–565.

Palmer AR & Russell IJ (1986). Phase-locking in the cochlear nerve of the guinea-pig and its relation to the receptor potential of inner hair-cells. *Hear Res* **24**, 1–15.

Parsons TD, Lenzi D, Almers W & Roberts WM (1994). Calcium-triggered exocytosis and endocytosis in an isolated presynaptic cell: capacitance measurements in saccular hair cells. *Neuron* **13**, 875–883.

Platzer J, Engel J, Schrott-Fischer A, Stephan K, Bova S, Chen H, Zheng H & Striessnig J (2000). Congenital deafness and sinoatrial node dysfunction in mice lacking class D L-type Ca^{2+} channels. *Cell* **102**, 89–97.

Pujol R, Lavigne-Rebillard M & Lenoir M (1998). Development of sensory and neural structures in the mammalian cochlea. In *Development of the Auditory System*, ed. Rubel EW, Popper AN, Fay RR, pp. 146–192. Springer-Verlag, New York.

Romand R (1983). Development of the cochlea. In *Development of Auditory and Vestibular Systems*, ed. Romand R, pp. 47–88. Academic Press, New York.

Rüsch A, Erway LC, Oliver D, Vennstrom B & Forrest D (1998). Thyroid hormone receptor beta-dependent expression of a potassium conductance in inner hair cells at the onset of hearing. *Proc Natl Acad Sci U S A* **95**, 15758–15762.

Rüsch A, Ng L, Goodyear R, Oliver D, Lisoukov I, Vennstrom B, Richardson G, Kelley MW & Forrest D (2001). Retardation of cochlear maturation and impaired hair cell function caused by deletion of all known thyroid hormone receptors. *J Neurosci* **21**, 9792–9800.

Steel KP & Bock GR (1980). The nature of inherited deafness in deafness mice. *Nature* **288**, 159–161.

Steel KP & Kros CJ (2001). A genetic approach to understanding auditory function. *Nat Genet* **27**, 143–149.

Steel KP & Smith RJ (1992). Normal hearing in Splotch (*Sp*/+), the mouse homologue of Waardenburg syndrome type 1. *Nat Genet* **2**, 75–79.

Vandenberghe W & Bredt DS (2004). Early events in glutamate receptor trafficking. *Curr Opin Cell Biol* **16**, 137–139.

von Gersdorff H, Sakaba T, Berglund K & Tachibana M (1998). Submillisecond kinetics of glutamate release from a sensory synapse. *Neuron* **21**, 1177–1188.

Vreugde S, Erven A, Kros CJ, Marcotti W, Fuchs H, Kurima K, Wilcox ER, Friedman TB, Griffith AJ, Balling R, Hrabe De Angelis M, Avraham KB & Steel KP (2002). *Beethoven*, a mouse model for dominant, progressive hearing loss DFNA36. *Nat Genet* **30**, 257–258.

Xie J & Black DL (2001). A CaMK IV responsive RNA element mediates depolarization-induced alternative splicing of ion channels. *Nature* **410**, 936–939.

Zhang LI & Poo M (2001). Electrical activity and development of neural circuits. *Nat Neurosci* **4**, 1207–1214.

Zheng J, Shen W, He DZ, Long KB, Madison LD & Dallos P (2000). Prestin is the motor protein of cochlear outer hair cells. *Nature* **405**, 149–155.

Acknowledgements

This work was supported by the MRC and Deafness Research UK. W.M. is a Royal Society University Research Fellow. We thank Jabulani Sithole for helping with statistical analysis, and Martin Hrabé de Angelis and Helmut Fuchs for the initial discovery of the *Beethoven* mutant.

Authors' present addresses

W. Marcotti: Department of Biomedical Science, Addison Building, University of Sheffield, Western Bank, Sheffield S10 2TN, UK.

S. L. Johnson: Department of Biomedical Science, Addison Building, University of Sheffield, Western Bank, Sheffield S10 2TN, UK.

K. P. Steel: Wellcome Trust Sanger Institute, Genome Campus, Hinxton, Cambridge CB10 1SA, UK.